GIMA
Geographical Information Management and Applications

Forced displacement in Mali

Analysing the effect of physical environment data on refugee flight routes in Flee

F. Boesjes
6228925

f.boesjes@students.uu.nl
March 4th, 2022

Supervision
dr. J.A. Verstegen (WUR)
kpt. B.J.H. Ooink (MinDef)

Responsible professor
dr. ir. R.J.A. van Lammeren (WUR)

Universiteit Utrecht
TU Delft
UNIVERSITY OF TWENTE.
WAGENINGEN UR
Ministerie van Defensie

Abstract

The twenty-first century has seen an increase in conflict-induced refugees (UNHCR, 2021). Understanding the refugee movements that result from these conflicts could aid policy makers and humanitarian organizations in providing aid to and hosting these forcibly displaced peoples (Suleimenova et al., 2017). To this end, Flee was developed (Groen, 2016). Flee is an agent-based social simulation framework for forecasting population displacements in an armed conflict setting (Anastasiadis et al., 2021; Suleimenova & Groen, 2020). Currently the flee-model does not take into account the possibility of refugees taking off-road routes. The goal of this study is therefore to implement into Flee the possibility for off-road driving routes, and test the effectiveness of these routes.

The off-road routes are determined by selecting features of the physical environment relevant to refugee movement, and representing these in raster data per season. Values are assigned to the selected features, to represent the degree of resistance that these features offer. The modelled resistance is changed to a cost raster, which allows for the plotting of routes of least cumulative resistance between two points. The resulting routes are used as input for Flee, in a Mali case study.

Overall, the model's refugee allocation error has decreased by 16.5% as a result of the changes in routes. However, most of this change is caused by an improvement of allocation in one camp, that influences the total through its relatively large size. When comparing the impact of the routes on the difference in error per location, while weighting the camps equally, the error increases by roughly 7%. Moreover, on a temporal level, the first and last season's error are lower due to border closure and camp capacity mechanics in Flee. The error in season two and three (April – Oct 2012) are thus the most reliable for testing the differences in model accuracy. These seasons show overall a negligible difference in error.

The study shows that the addition of routes based on the physical environment does improve the overall accuracy of Flee's refugee allocation in the Mali case study, but the results are too inconsistent to determine whether this will be the case in other case studies as well. Other factors are the root cause of current differences between the model and reality. These root causes include for example political factors, such as border restriction policies, and decision-making based on emotional factors, such as the attractiveness of cities over refugee camps.

Table of Contents

Acronyms

Commonly used acronyms in this document:

ACLED - Armed Conflict Location & Event Data Project

DSM – Digital Surface Model

ESA – European Space Agency

FDP – Forcibly Displaced People

GEE – Google Earth Engine

JAXA – Japanese Aerospace Exploration Association

NDWI – Normalized Difference Water Index

NIR – Near-Infrared

OSM – Open Street Map

SWIR – Short-wave infrared

WiW – Water in Wetlands

1. Introduction

The twenty-first century has seen an increase in refugee numbers (UNHCR, 2021). The previous years were no exception to this. Due to crises in Venezuela, Syria, Afghanistan, South Sudan, Myanmar and many other locations, this number increased to roughly 82.4 million forcibly displaced people (FDP) in 2020 (Figure 1). This amounts to some 1 in 95 in terms of world population, according to the United Nations High Commissioner for Refugees (UNHCR, 2021). Furthermore, although empirical evidence is lacking, a changing climate might further increase the risk of conflict, especially in developing countries (Abel et al., 2019; Mach et al., 2019). Understanding the refugee movements that result from these conflicts could aid policy makers and humanitarian organizations in providing aid to and hosting these FDPs (Suleimenova et al., 2017).

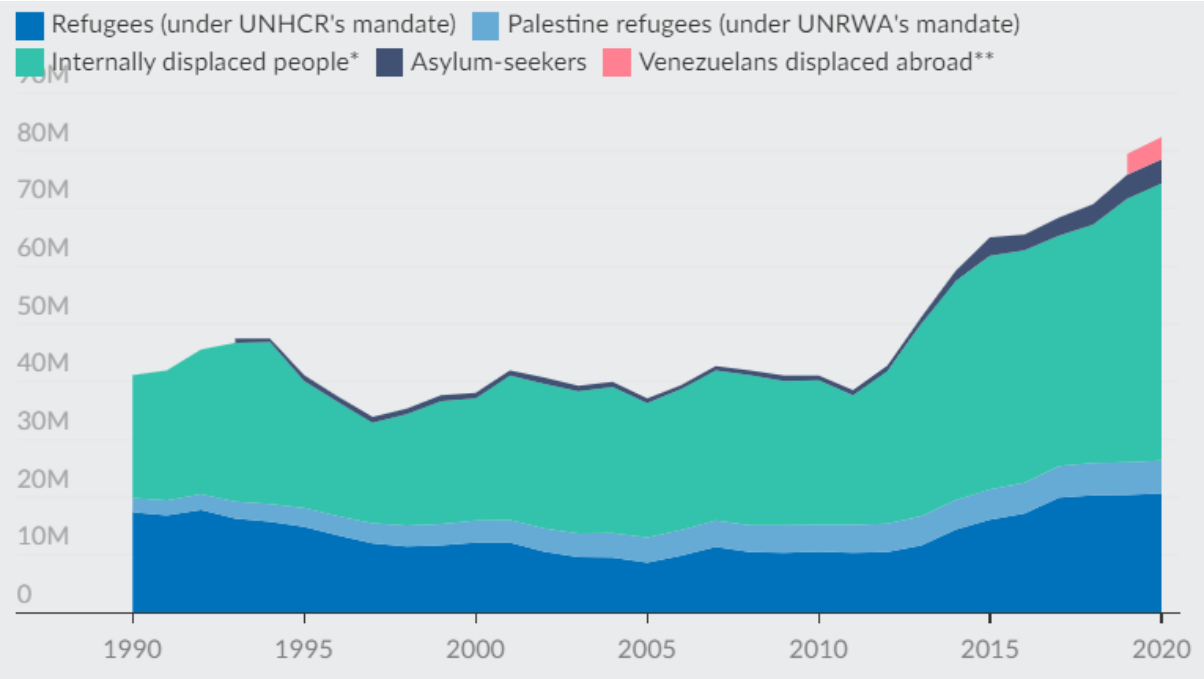

Figure 1: UNHCR Forcibly Displaced Peoples statistics. Source: UNHCR, 2020.

Several studies were performed on simulating refugee movements on a city or community wide scale (Anderson et al., 2007; Sokolowski et al., 2014, 2015). Furthermore, several frameworks for aiding the creation of computational refugee models have been developed (De Kock, 2019; Searle & Van Vuuren, 2021). On large-scale migration modelling, mainly international migration, many papers have been written (Stillwell, 2005). However, in terms of computational studies on the movements of refugees in an armed conflict setting on a national scale, little has been done. To this end, Flee was developed (Groen, 2016). Flee is an agent-based model used for simulating population displacements in an armed conflict setting (Anastasiadis et al., 2021; Suleimenova & Groen, 2020). In agent-based modelling, a system is simulated as a collection of autonomous decision-making entities, known as agents (Bonabeau, 2002). In the Flee model, these agents represent refugees. The agents in Flee are tied to a network: starting from a node, which represent for example a town or a refugee camp, and travelling across connections to other nodes. In Flee, connections between nodes are determined by the presence of a road connection. Which node the agents decide to travel to is decided by their simulated level of knowledge of the area and a 'move chance', which is decided by several factors (Anastasiadis et al., 2021; Groen, 2016).

Flee has already been tested on a number of case studies (Suleimenova et al., 2017). One of these case studies is the conflict in Mali. In 2012, a civil war erupted in Mali in which several separatist and Islamist groups fought for the independence of Azawad, the northern part of the country (Bencherif et al., 2020; Shaw, 2013). To counteract the destabilization of the already vulnerable region, the French responded with military intervention, after which the United Nations followed suit (Lounnas, 2013). In its nine year duration, the conflict has led to hundreds of thousands of displaced people and to some

fifty thousand currently (R4Sahel, 2021; UNHCR, 2021). This conflict was reproduced in Flee in 2016 by D. Groen, as part of the development of Flee (Groen, 2016). The model has shown promising results in terms of accuracy. For example, Flee has managed to reproduce the key refugee movement patterns in several case-study conflicts, including Mali, and has correctly simulated at least 75% of refugee destinations for these case studies after the first 12 days of the conflict simulation (Suleimenova et al., 2017).

However, many aspects that might determine refugee flight behaviour and destinations are still not taken into account in Flee (Suleimenova & Groen, 2020). Among these are aspects of the physical environment. Mapping and classifying the physical environment allows for simulating the paths that people most likely take towards their destination when clearly discernible roads are absent, or when existing roads have become inaccessible. Currently, Flee does not take into account the possibility of refugees taking off-road routes. However, experience from the Ministry of Defence has shown that a significant amount of travel in Mali occurs via such routes (B. Ooink, personal communication, September 2021). Furthermore, testing with the Flee model has shown that the addition of off-road walking routes can significantly decrease the validation error (Suleimenova & Groen, 2020). Therefore, it could be essential for the accuracy of the model and the eventual allocation of humanitarian resources to represent these routes in the simulation.

1.1 Research Objectives and Questions

The problem that this study seeks to address can be formulated as follows: 'Current refugee simulation through the Flee model does not include aspects of the physical environment or off-road flight routes.'

The general aim of this study is therefore identifying to what extent aspects of the physical environment affect refugee flight behaviour, and would therefore improve the Flee model's simulation of refugee behaviour. The secondary aim to this study is to improve the accuracy of the Flee model.

The main research question related to these objectives is:

'To what extent does the physical environment determine flight routes for refugees?'

The sub-questions that aid in answering this question are:

1. To what extent does a representation of the physical environment approach accurate refugee travel times and distances?
2. What is the effect of the integration of the cost raster data on the spatial aspect of the projected refugee destinations of the Flee model's simulations?
3. What is the effect of the integration of the cost raster data on the temporal aspect of the projected refugee destinations of the Flee model's simulations?

The first of these questions addresses effect of the route implementation on the spatial aspects of the Flee simulations. The physical environment in this question pertains to features of the environment relevant to refugee mobility. The goal of this question is to find out if a spatial pattern exists in the model output, and how these patterns differ before and after the implementation of the new routes. The second question addresses the same issue, but related to the time factor of Flee, instead of the geographical factor. The goal for this question is to discover patterns in differences between seasons, and what effect the seasons might have on the refugee simulation results of Flee.

2. Background

2.1 Agent-based Modelling

In understanding complex geographical and social problems such as sprawl, migration, congestion, segregation and many others, researchers have traditionally turned to relatively static and aggregate explanations for these systems. However, as geography became a science with a more heterogeneous approach, so did its methods of research (Crooks & Heppenstall, 2011). One of these methods is called agent-based modelling. Agent-based modelling, or ABM, is a simulation method with the goal of simulating a system or network in a bottom-up manner. However, many different approaches to, and definitions of ABM exist, so it might be more of a mindset than a technology (Bonabeau, 2002).

In recent years, ABM has become a popular simulation approach for scientists studying social interactive systems and networks (Suleimenova et al., 2017). It allows for a decentralized approach to explaining these systems using agents. Agents are individual, active objects that behave heterogeneously within the simulated system. Bonabeau (2002) describes them as 'autonomous decision-making entities'. Agents act according to a basic set of rules, but all in a slightly different manner (Crooks & Heppenstall, 2011; Macal, 2016). An agent assesses its unique situation on these basic rules and executes various behaviours accordingly (Bonabeau, 2002). This heterogeneous behaviour allows for arguably the most valuable aspect of ABM, which is simulating and describing emergent properties and situations. Other benefits of ABM are that it provides a natural description of a system and that it is a flexible method (Bianchi et al., 2007; Bonabeau, 2002).

Roughly speaking, ABM knows two categories of use: explanation and projection. Explanation serves to understand past observations of a system or parts of a system (Crooks & Heppenstall, 2011). Projection on the other hand is used for 'extrapolation of trends, evaluation of scenarios, and the prediction of future states', according to Castle & Crooks (2006). In this category, ABM are useful for example for simulating scenario development and the effects of policy or behavioural changes. This use of ABM should not be interpreted as a way of predicting a situation perfectly, but as a way of projecting what a situation might entail, always with a margin of error. Therefore, the term projection instead of prediction is used in this study.

2.2 The Flee Model

The Flee model is an example of an agent-based model. More specifically, it has been called 'an agent-based social simulation framework for forecasting population displacements in an armed conflict setting' (Anastasiadis et al., 2021). Groen (2016), the initial developer of Flee, mentions three reasons for the creation of Flee. First, the usage of refugee simulations allows for estimating the effects of changes in border and migration policies, which helps in informing governments and the general public about the consequences of such changes. Second, simulations help project where refugees are most likely to go under certain circumstances, when a conflict erupts. This could allow humanitarian and support organizations to prepare for these situations. Third, current empirical data on refugees is incomplete. The nature of refugees makes it difficult to accurately and consistently collect data on them (Suleimenova et al., 2017). Simulations could help fill the gaps in these data, and make projections when no data is available. Furthermore, running simulations is not restrained by ethical considerations that are requisite in social empirical studies and experiments.

As in any agent-based model, the setting in which Flee simulates refugee movements is defined by inputs, parameters and agents. In Flee, agents represent refugees. The amount and location of refugees that are used in the model is dependent on real-world data. These data are taken from the UNHCR database, which consists of empirical data that are collected at refugee camps in the region (UNHCR, 2021). The simulated setting represents the outbreak of an armed conflict, which leads to refugees flowing out of the location of the conflict, and towards refugee camps. This setting is created by other input data, such as routes, locations of towns, cities and camps, conflict locations and conflict outbreak dates and finally border closure dates and locations. In Flee, the assumption is made that refugees stick to major roads in their flight. The routes are therefore derived from Bing maps, which is used to estimate the travel distance using the shortest routes planned for vehicles. The assumption is made as well that refugees travel by car (Groen, 2016).

3. Methodology

3.1 General methodology

In this section, a general overview of the used methods and the order in which they are applied is given, and visualized in Figure 2.

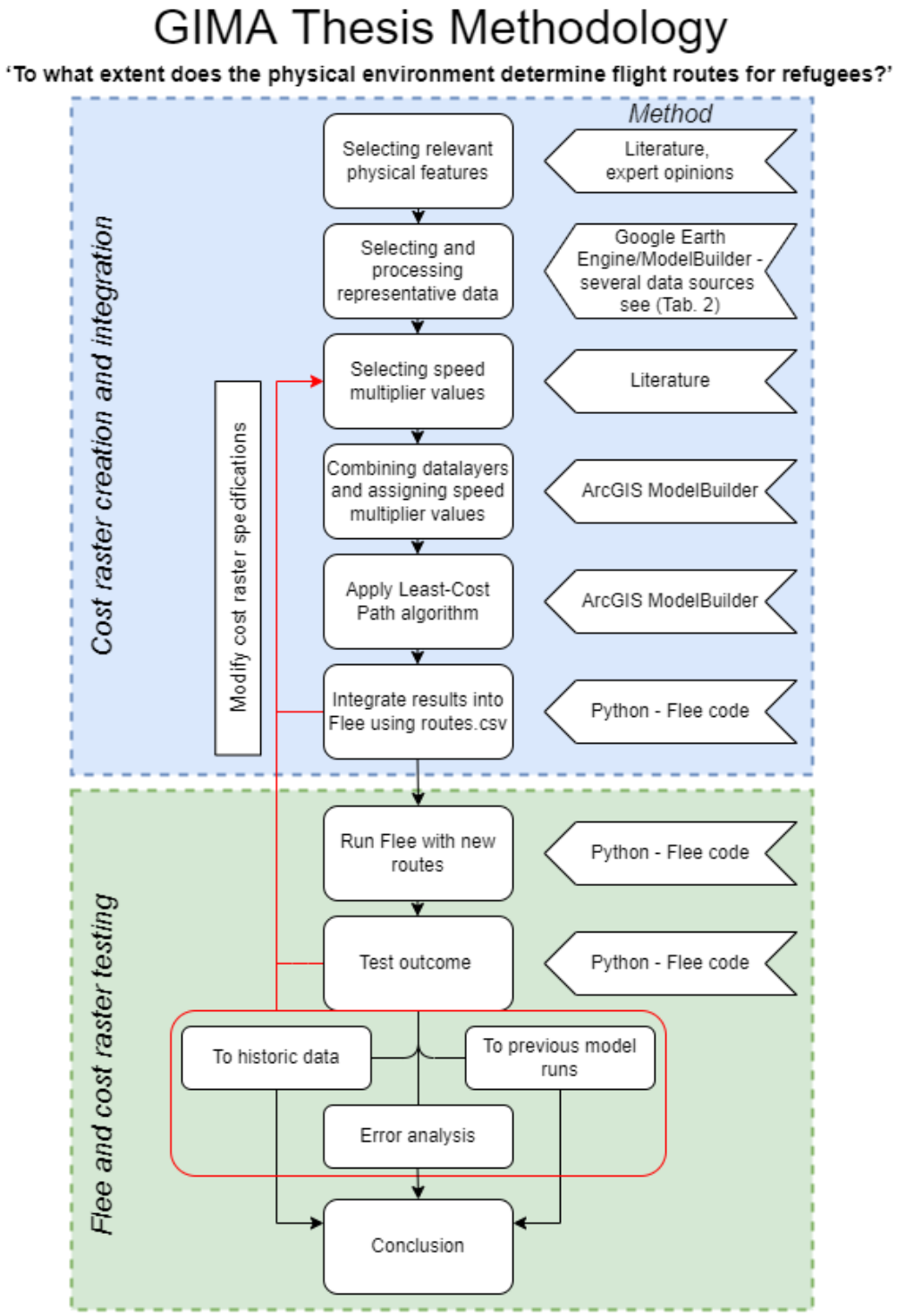

Figure 2: Schematic overview of the cost raster creation methodology.

The first step in creating the cost raster is to select the relevant physical features and representative data (section 3.7). The second step is to define speed multiplier values, determining the relative resistance for each of the geographic features. The values are determined through literature research (section 3.8). After the selection of features, data and speed multiplier values, the values are applied to the datasets, which are in turn combined into the cost raster (section 3.3) (Figure 2).

After the cost raster has been completed, the next step is to create new routes using the Least-Cost Path algorithm (section 3.4). These routes are used in the Flee model. After the completion of model runs including the new routes, the outcomes, consisting of refugee numbers per destination, are compared to earlier model results. The results are validated and discusses using descriptive methods and several methods of error analysis (section 4). Finally, a conclusion is drawn (section 5).

3.2 Flee initialization

The core parameters of Flee specify the environment of the conflict, the population of agents and their properties, which form the basis of their behaviour (Anastasiadis et al., 2021). Population is defined by the initial number of agents and the number of new agents added to the population per time step, which is derived from UNHCR input data (2021). The numbers of refugees that are added in the model are based on the data from the UNHCR (2021).

The movement of the agents is calculated on a daily basis, and is parameterized by a *movechance*, which equals 1 in source locations, or where the conflict takes place, indicating a 100% chance that the agent moves away from that location (Groen, 2016). The movement is limited by the total number of simulation days (*simulation_days*), the maximum movement speed of the agents per day (*max_move_speed*), and the level of awareness (*AwarenessLevel*), which marks the distance an agent takes into account when deciding on a destination to move to. The agents are inserted in the simulation in locations, or nodes, which represent for example towns. The movement behaviour of the models' agents is defined by a set of behavioural rules. The agent moves with 100% chance if the agent is located on a conflict node (*conflict_move_chance*). If the agent is in a camp (*camp_move_chance*) or another location (*default_move_chance*), the move chance is 0.1% or 30% respectively (Suleimenova et al., 2017). Destinations are picked by agents according to location weights (*camp_weight*, *conflict_weight*). Each timestep agents make their choices based on the chances mentioned above, and move with a maximum of 200km/day (*max_move_speed*). Of these parameters, all default values are mentioned in Table 1. If all agents have made their choices, the timestep is increased and the agents move a certain distance towards their location, and the process repeats. The flow of this process is visualized in Figure 3.

Table 1: Description and default values of input parameters. Source: Suleimenova et al., 2017.

Parameters	Description	Default value
max_move_speed	Agents' maximum movement speed in the simulation while traversing between locations.	200 km/day
simulation_days	The amount of days that the simulation runs for.	300
AwarenessLevel	0 represents current route only, not knowing the destination; 1 represents knowing the destination as well; 2 represents knowing the surrounding routes and locations; 3 represents awareness of the region, which includes several locations and routes.	1
camp_move_chance	Probability of an agent moving from camp location where an agent resides to another location (on a scale of 0 to 1).	0.001
conflict_move_chance	Probability of an agent moving from conflict location where an agent resides to another location (on a scale of 0 to 1).	1.0
default_move_chance	Probability of an agent moving from other (default) location where an agent resides to another location (on a scale of 0 to 1).	0.3
camp_weight	The attractiveness value for camp locations making them twice as likely to be chosen as destination (relative to 1).	2.0
conflict_weight	The attractiveness value for conflict locations making them four times less likely to be chosen as destination (relative to 1).	0.25

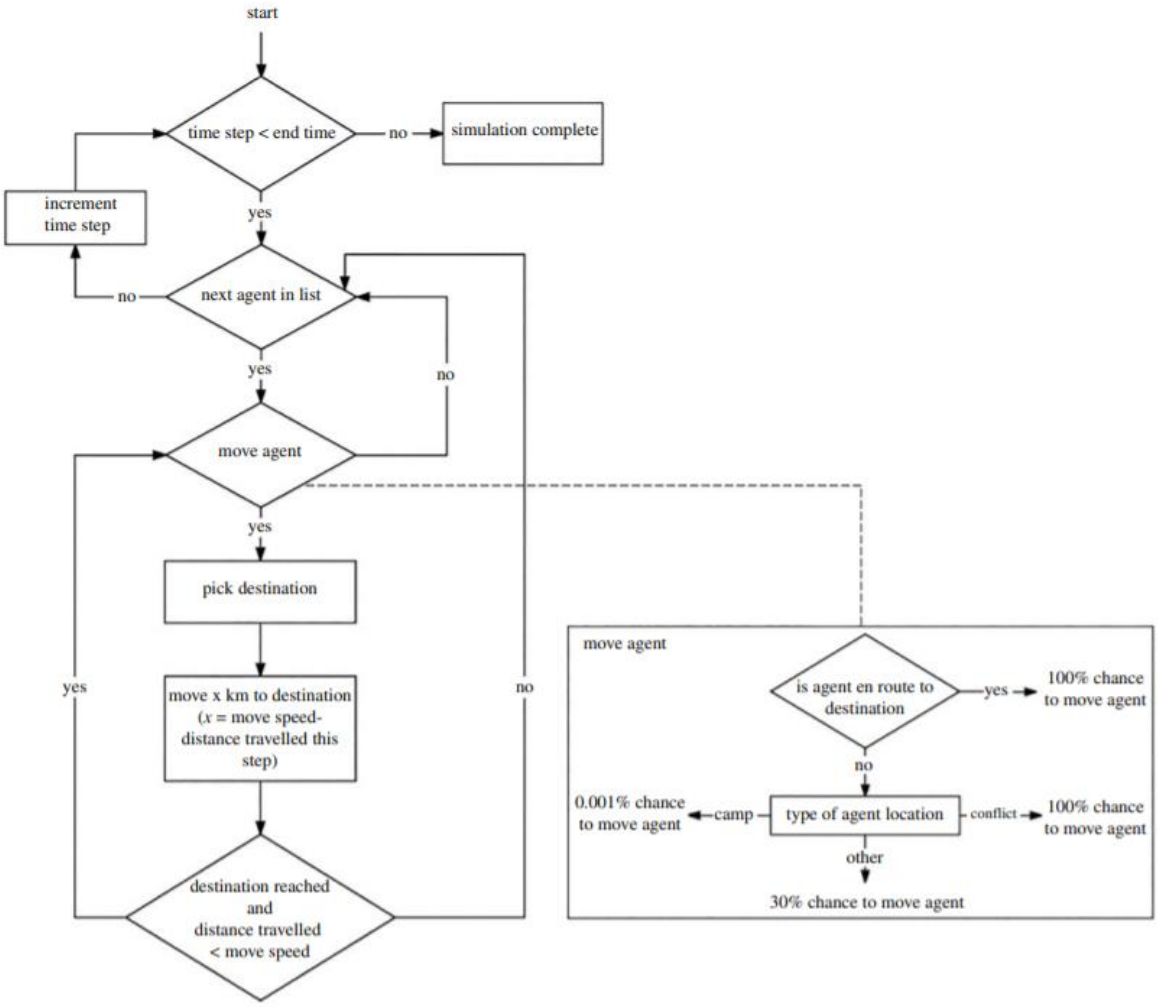

Figure 3: Flee model agent behaviour flowchart. Source: Suleimenova & Groen, 2020.

The possible routes an agent might take are decided by the input of routes files (routes.csv), and the destinations are formed by nodes, which represent refugee camps, cities, conflict zones, forwarding hubs, etc. The routes and destinations combined form the 'location graph' or 'network graph' (Anastasiadis et al., 2021). Camps are assigned a maximum capacity of refugees. When the camps approach reaching this capacity, the weight of the attractiveness of these camps is reduced. Capacity can briefly be exceeded, but is eventually avoided as a destination (D. Groen, personal communication, February 2022). Flee also has access to applying border closures into the model. The border closure starts at a set time, and prevents any agents from travelling to locations in the closed-off region. An example of the location graph for the original Mali case study can be found in Figure 4.

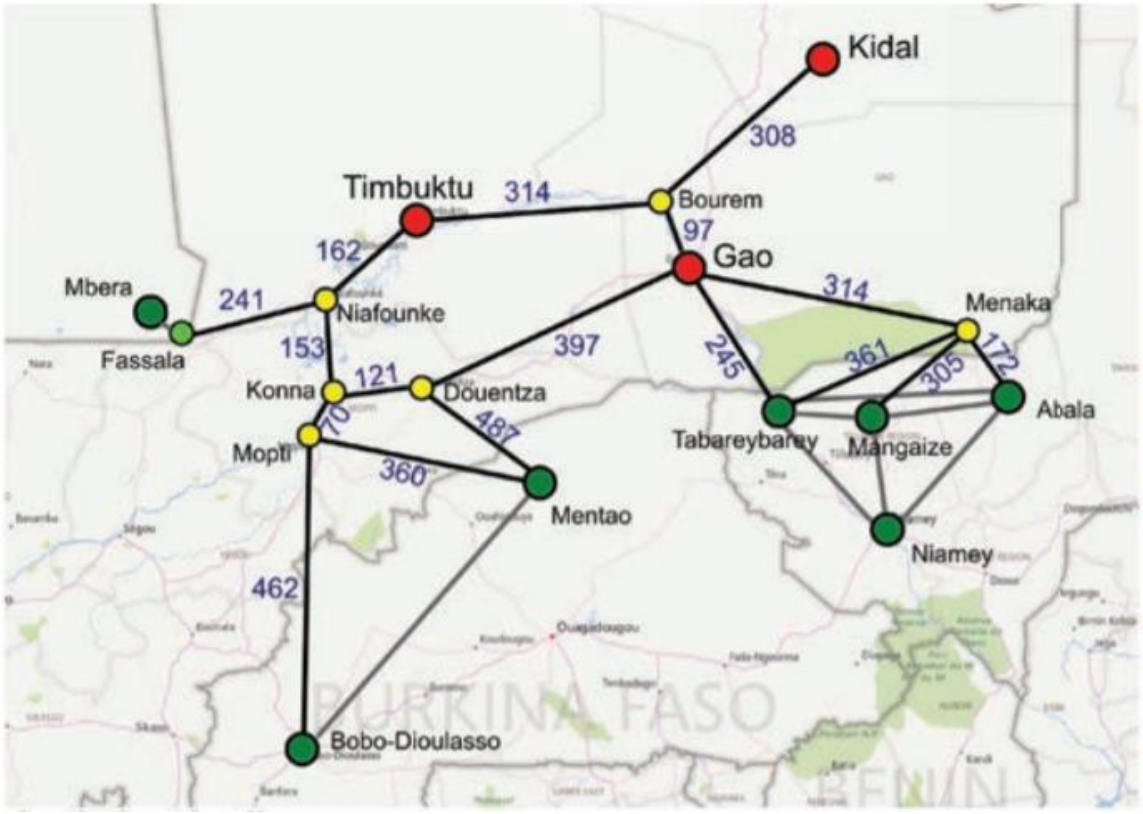

Figure 4: Overview of the simulation model. Source: Groen, 2016.

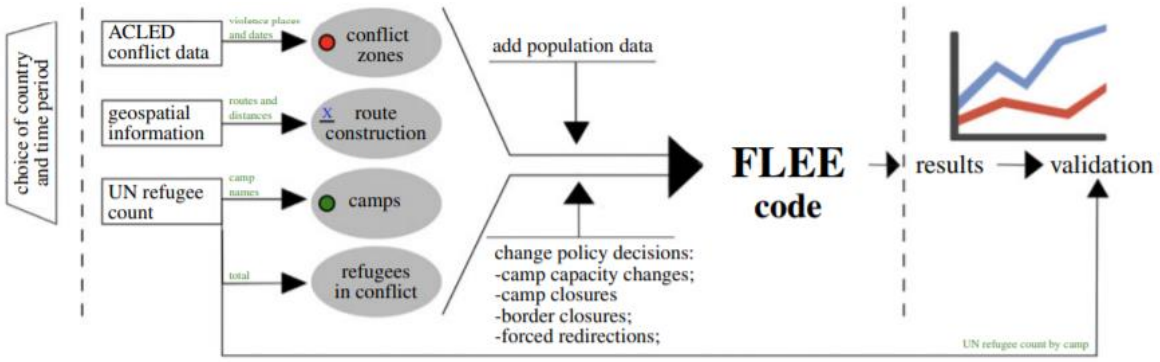

Figure 5: Visualization of the general workings of the Flee model. Source: Suleimenova & Groen, 2020.

In chronological order, Flee is set-up as follows. The first step is the setting of inputs, which consists of conflict, refugee and route data. Next, the setting of parameters and the running of the model leads to results. These result are verified to determine if the model works as expected, and validated to determine the accuracy of the results (Figure 4).

The changes that are made to Flee in this study pertain mainly to a single element of the model, which is the route construction (Figure 5). Currently in Flee, all routes are based on the availability of connections in Bing Maps. In this study, the physical environment is represented in the form of a cost raster, from which routes can be determined using Least-Cost Path analysis, based on the Dijkstra algorithm (Choi et al., 2013; Murekatete & Shirabe, 2020) (section 3.3). The routes that are derived using this method, are used as alternative routes to the Bing Maps routes in Flee. In this way, when Flee is run, it uses routes that take into account the physical environment as well, and not just roads (section 3.6.2). Figure 5 shows the Flee model in chronological order from left to right.

The implementation in Flee is done by exporting the routes as a 'routes.csv' file. These files are the input that determine the connections in the network graph available for agents to traverse. These input files are comprised of four columns of data*: Name1, Name2, Distance[km]* and *forced_redirection*.

Location A and B mark the start and end point of a route respectively. *Distance* displays the distance property of the route, but is also used as a weighting factor. For example, if one would want to simulate that travel on a route takes twice as long, due to traffic congestion for instance, this distance value would be doubled. The *forced_redirection* column refers to a redirection from a source location, which can be a town or a camp, to a destination location. The source location is then indicated as forwarding hub. In this column, the value 0 indicates no redirection, 1 indicates redirection from *Name2* to *Name1,* and 2 indicates redirection from *Name1* to *Name2*. The implementation of the new routes, which take into account the seasonal changes in weighted route length, require the splitting-up of the *Distance* column into four seasons. D. Groen, the developer of Flee, has updated the Flee code to allow for this. With this update, the connection between two locations can differ in length between seasons. A schematic overview of this file structure, and the change that is made therein, can be found in Table 2 and 3.

Table 2: Routes.csv original file structure.

Name1	Name2	Distance	Forced_redirection
A	*B*	*X1*	*0*
B	*C*	*X2*	*1*

Table 3: Routes.csv adapted file structure.

Name1	Name2	DistanceS1	DistanceS2	DistanceS3	DistanceS4	Forced_redirection
A	*B*	*X11*	*X12*	*X13*	*X14*	*0*
B	*C*	*X21*	*X22*	*X22*	*X24*	*1*

3.3 Cost Raster creation

To create the routes, first a cost surface needs to be created. Such a surface represents the cost of travel across a region, represented as raster data. To do this, first a representation of the physical environment of Mali is made. This is done by selecting data relevant to refugee travel, and representing these data as unique values in a raster dataset. Then, speed multiplier values, which range between 0 and 1, are assigned to these unique values, creating the multiplier raster. These speed multiplier represent inversely the resistance that the selected physical features offer, meaning high values indicate low resistance. The complete multiplier raster is then multiplied by a speed value, in km/h. This allows for easily testing different speed values and calibration of the raster and eventual routes. The output of this multiplication is named the speed raster, representing the maximum driving speed that each unique physical feature allows. After the speed raster is finished, the values are recalculated into costs, in hours per meter. The main difference of the speed and cost raster is that in a speed raster, high values represent faster travel, while in a cost raster, low values represent faster travel. This is needed for the least-cost path operation for the creation of routes, where routes are determined based on the least cumulative cost. This cumulative cost then represents for each route the time it takes to travel that route in hours. This process is schematically visualized in Figure 6.

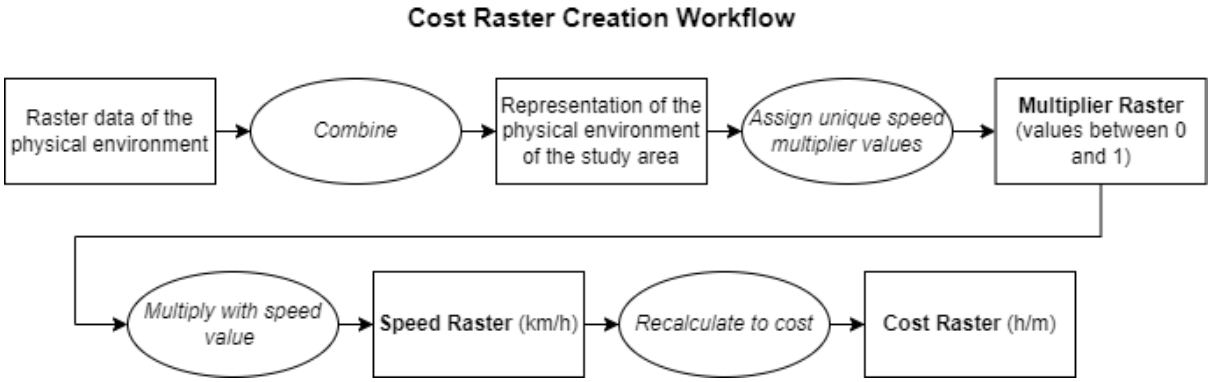

Figure 6: Conceptual workflow for the creation of the cost raster.

In representing the physical environment, choices need to be made as to what features are included in the representation.

The features used in this study are selected to represent the features of the physical environment that are relevant to a refugee. This selection is based on a classification used by NATO to denote the composition of the physical environment as it is relevant to human mobility. The classification is compromised of *Relief, Drainage, Soil, Vegetation and Infrastructure.* These five factors are deemed the most influential to human mobility by the Ministry of Defence (B. Ooink, personal communication, September 2021). As flight behaviour is treated as a matter of mobility, these factors are used as a guideline in determining features that are relevant to refugees as well. Due to time constraints, *Vegetation* is not taken into account for this case study. From different classes, this one is deemed the least relevant in the situation of Mali.

The *Soil* data, in this case more accurately represented by the term surface, is split between rocky areas, bare and rest areas. The *rocky areas* class is derived through a random forest supervised classification of satellite images. This method is proven to yield accurate results when used for defining land cover classification (Gambill et al., 2016; Gislason et al., 2005) The *rocky areas* class is meant to delineate a phenomenon in Mali where patches of sharp, jagged rocks cover the surface. From personal communication it is found that these surfaces are virtually impassable for civilian vehicles, as the rocks have the ability to destroy tires (B. Ooink, personal communication, September 2021). These dark patches are distinguishable from space. Therefore, random forest supervised classification allows for sharp demarcation of these areas. The rocky areas are set to *NoData*, using the *Set Null* tool, where the presence of rocks is set to *NoData*. This allows for further calculations to take place, without taking into account the rocky areas, as these are untraversable. To the bare and rest dataset a speed multiplier (*ResVal*) class is added. These classes are defined through a reclassification of a predefined land.

Drainage is represented by the presence of water or wetlands. For the water and wetlands data the seasonal presence of water is set to *NoData*, to represent an impassable surface. The yearly dataset denotes the locations of dried up wetlands, or floodplains. The cells of this dataset are set to the determined speed multiplier values as well. The water data is derived using the Normalized Difference Water Index. In remote sensing, NDWI may refer to several different indexing methods. In this study, the method proposed by McFeeters (1996) is used. This method is created specifically to delineate land from open water using light in the green and near-infrared (NIR) wavelengths (Eid et al., 2020). Moreover, a study by Özelkan (2020) has shown that the NDWI method proposed by McFeeters (1996) is the most suitable method for detecting water bodies in comparison to several other methods developed for this purpose. The formula for McFeeters' NDWI posed in Equation 1.

$$NDWI = \frac{(Green - NIR)}{(Green + NIR)}$$

Equation 1: NDWI calculation.

The NDWI yields a dataset with values between 1 and -1. As a general rule, positive values depict water (Özelkan, 2020; Rokni et al., 2010; Sarp & Ozcelik, 2017). This is caused by the relatively high reflectance of NIR light by soil and terrestrial vegetation (McFeeters, 1996).

While the NDWI is ideal for detecting open water bodies, it is not suitable for measuring moisture levels in soil. This means the index cannot be used for measuring wetlands. In general, the remote sensing of wetlands provides a difficult challenge to researchers (Mahdavi et al., 2017). This is mainly due to the dynamic nature and ambiguous definition of wetlands (Gallant, 2015). Wetlands constantly change, as many wetland areas flood periodically and vegetation is quick to change in such areas (Rundquist et al., 2001). Furthermore, measuring moisture levels under an obstructing layer of vegetation is challenging indeed. However, a relatively new method, published in 2019 by Lefebvre et al. (2019), provides a new approach. The *Water in Wetlands* (WiW) method uses a relatively simple calculation to distinguish wet- from dryland (Equation 2).

$$Wetland = NIR \leq 0.1804 \,\&\, SWIR \leq 0.1131$$

Equation 2: Wetlands selection formula. Source: Lefebvre et al., 2019.

In Equation 2, near-infrared (NIR) and shortwave-infrared (SWIR) are combined. SWIR is used, as it is sensitive to moisture both in soils and in vegetation (Lefebvre et al., 2019; Mahdavi et al., 2017). If the reflectance value of a pixel is lower than 0.1804 in the NIR band, and it is lower than 0.1131 in the SWIR band, the pixel should be classified as wetland. The values in this formula are specified to best suit Sentinel 2 data. To apply the NDWI and WiW methods, satellite imagery that includes at least RGB, NIR and SWIR bands should be used.

Infrastructure is split into roads, which is in turn split into five types, and river crossing, of which three types are classified. River crossings are buffered by 45 meters, resulting in a diameter of 90 meters around the river crossings, or roughly three cells. This is done to prevent connections getting lost in future data transformations, mainly from vector to raster data. The roads and river crossing data are subsequently assigned their speed multiplier values. The result is eight raster datasets representing the infrastructure: five rasters depicting several types of roads, and three rasters depicting river crossings. To use these data correctly in the model, some assumptions had to be made:

1. Due to the periodically low water level, ferries are only usable in high river levels;

2. Due to the periodically high water levels, fordable areas are only usable in low river levels;

3. Bridges are always usable.

The relations between the infrastructure and the seasonally differing environment mentioned above are represented as such in the model.

After the datasets are in their correct state, they are added together using several operations. In the initial situation, all cells in the study area are valued at 1. The first step is to subtract all impassable

surfaces from the area. This is done by multiplying the 'Value1' dataset by rocky areas and seasonal water and wetlands.

The next step is to assign speed multiplier values to the remaining cells. First the land cover data is taken into account, by multiplying the speed multiplier values with the previously created raster. Now all cells have either a *NoData* or land cover speed multiplier value. After this, the yearly wetlands are added by replacing the previous speed multiplier values if the floodplain value is lower. Where no floodplains are present, the land cover speed multiplier value is used. Finally, the roads are overlaid, ignoring the previous operations when a road is present, and assigning the road speed multiplier value to the cell.

Representing *Relief*, the final step is to assign the slope speed multiplier values, as these affect roads as well. Slope data is derived from a digital elevation model, a DEM, and represents the percentage of incline between different elevations. The aspect, or the orientation of the slope, is not taken into account when deciding the degree of resistance that the slope offers. The slope data is reclassified into five classes, each with their own speed multiplier value. However, as the slopes directly influence speed, first the cells have to change from an arbitrary speed multiplier value to km/h. This is done by multiplying the entire raster by a maximum speed value. When the cells represent speed, they are adjusted to the speed multiplier effect of the slope, in accordance with the assigned speed multiplier classes. The speed raster is now finished.

Finally, the speed raster, representing the maximum speed that might be driven in a cell, is converted to a cost raster, representing the time it takes to travel one meter in the cell. This is done using the following Equation 3.

$$Cost = \left(\frac{1}{SpeedValue}\right) * 0.001$$

Equation 3: Cost raster formula

In Equation 3, *SpeedValue* is the speed value assigned to each cell of the raster. The formula returns the cost in hour/meter. The transformation to cost raster is necessary for the Least Cost Path operation.

To finalize the creation of the cost raster, the raster is resampled from a horizontal resolution of ~30x30m to 100x100 meters, while using the minimum value of the aggregated cells. This method ensures that roads and river crossings remain represented in the raster. The resampling is performed to reduce processing time and storage requirements.

For the creation of the cost raster, the ArcGIS Pro ModelBuilder is used. This tool allows for easy adoption of changes and repetition of the model. Furthermore, it provides a visual overview of the complete model. A schematic overview of these steps, including the details of the operations, can be found in Figure 7. The details are further on described individually.

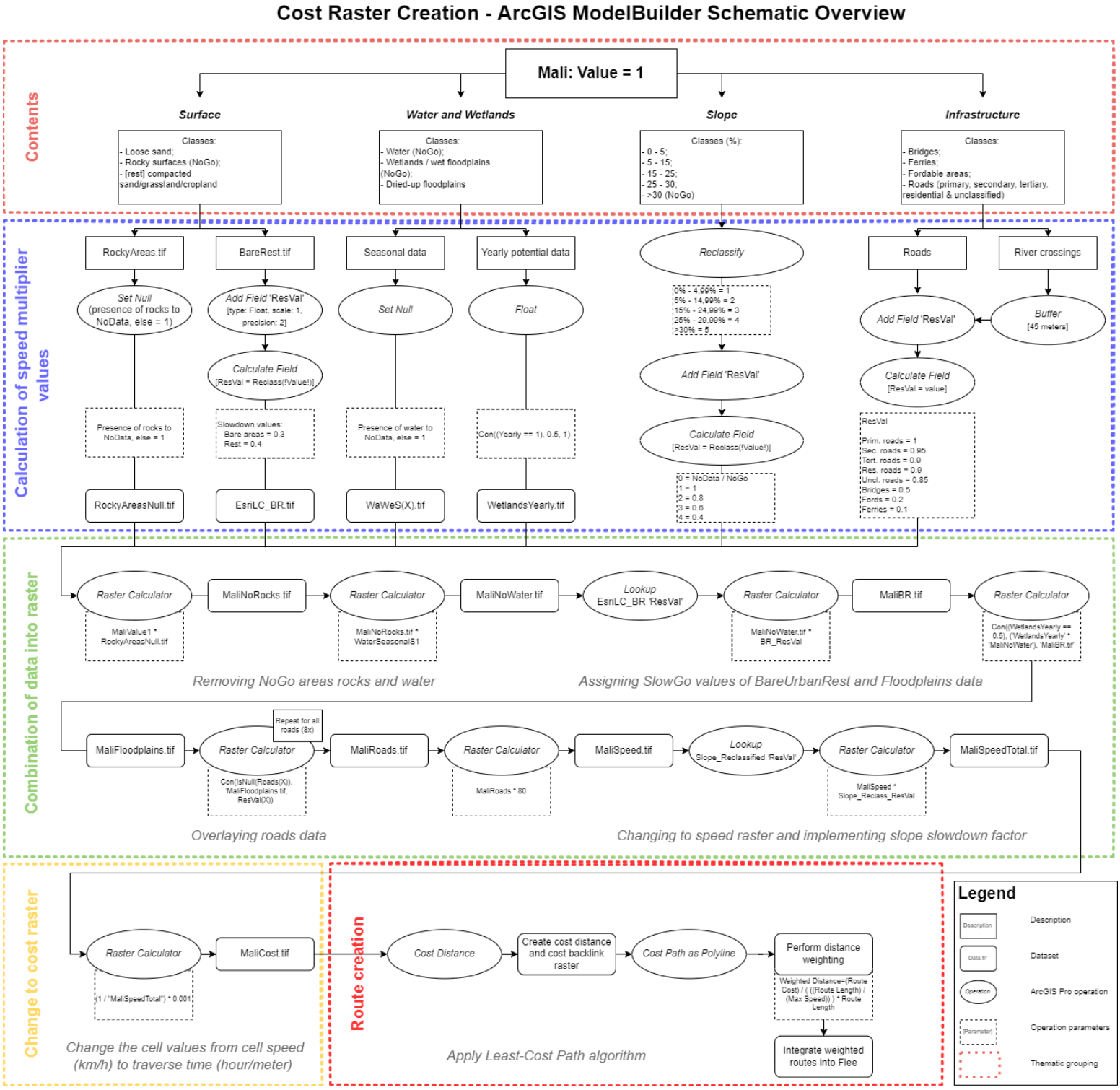

Figure 7: Schematic overview of cost raster creation.

3.4 Route creation and implementation

To create the routes, the data are transformed to a projected coordinate system that uses metric units, in this case meters, as map units. In this study all data use the geographic coordinate system WGS 1984, and the corresponding datum D WGS 1984. To minimize projection-induced distortion, the projected coordinate system WGS 1984 Web Mercator (Auxiliary Sphere) is chosen. This system uses the same datum as the geographic coordinate system WGS 1984, and therefore does not require a datum change. Furthermore, the Mercator projection increasingly distorts land area and distance towards the poles, but remains accurate around the equator, which is where the study area is located.

To create the routes, first, start points and destinations have to be defined. Relevant locations are defined using UNHCR data. Which locations are connected by routes are defined using data on existing road connections and local knowledge of the region. Which locations and routes are used in this study and why is described in section 3.6.5.

To create least cost path routes across the created cost surfaces, two additional raster have to be created per route: a backlink raster and a cost distance raster. Both can be created using the Cost Distance tool in ArcGIS Pro. This tool requires two inputs: the cost surface and the source data, or start location. The cost distance raster identifies, for each cell, the least accumulative cost distance over a cost surface to the identified source location, where the cost is measured in hours per meter. The resulting raster therefore contains data for each cell on the least cost, not Euclidean distance, to the source location (Figure 8). Examples of both rasters are found in Figure 8 and 9, using Ségou as source location.

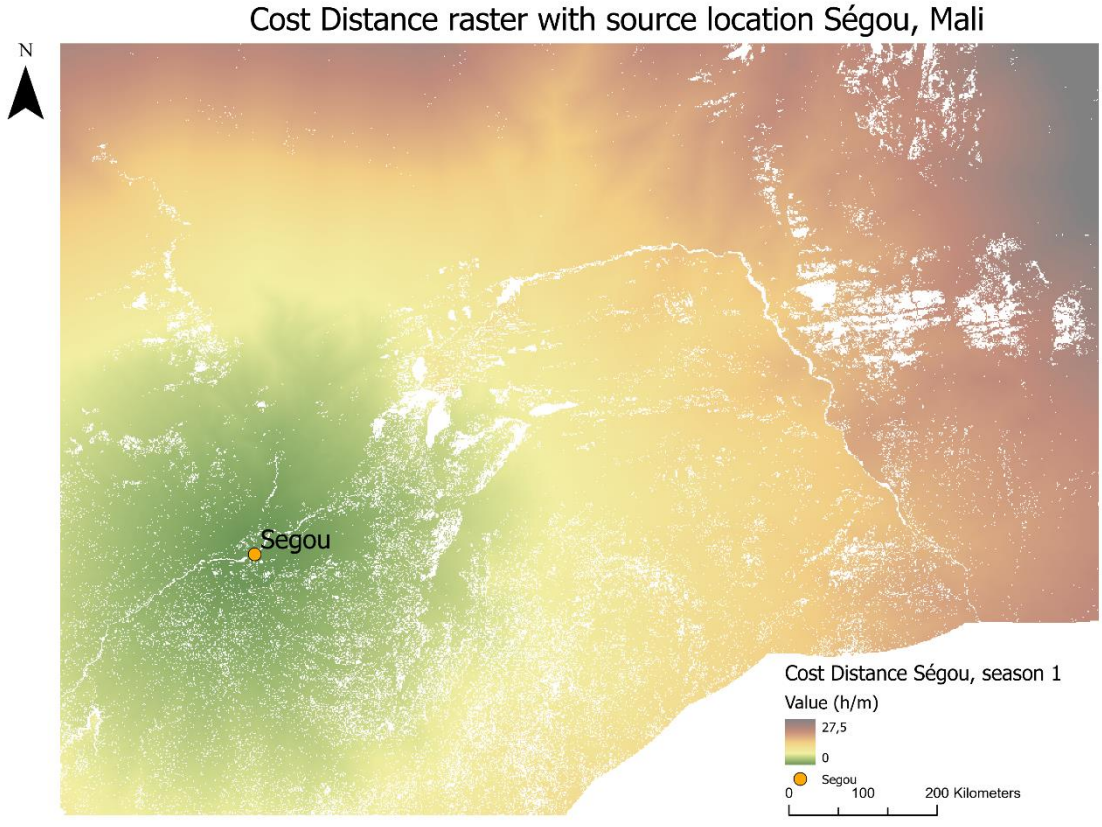

Figure 8: Cost Distance raster for Ségou, Mali.

The backlink raster defines the direction or identifies the next neighbouring cell along the least accumulative cost path from a cell to reach its least-cost source. It contains values ranging from 0 through 8, each representing a direction (right, lower-right, down, etc.) (Figure 9).

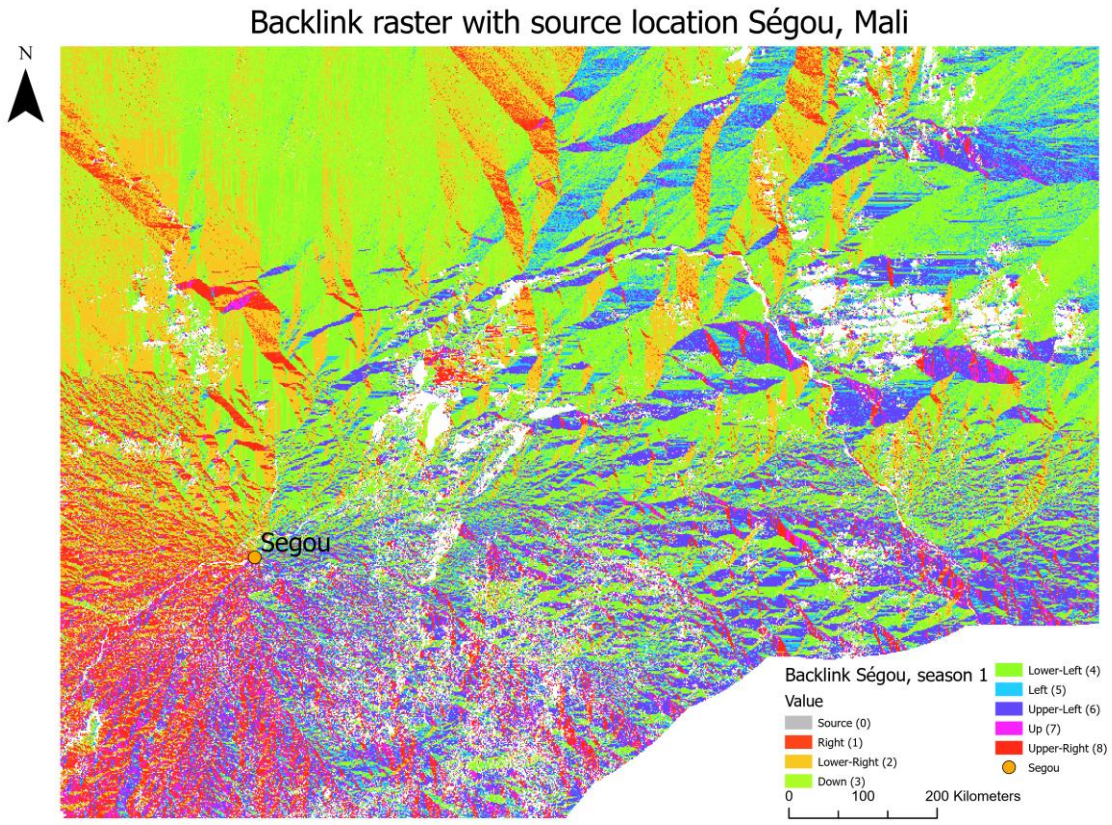

Figure 9: Backlink raster for Ségou, Mali.

When these rasters are created, the calculation of the least-cost path can begin. The tool used for this is the Cost Path as Polyline tool in ArcGIS Pro. This tool takes three datasets as input: the destination point data, a cost distance raster and a backlink raster. The tool calculates the least-cost path between the source cell used for creating the cost distance and backlink rasters, and a destination, defined here. The tool returns a polyline feature, with an attribute representing the accumulative cost of the represented route, in this case in hours.

The final step is to transform the cost of the routes to a weighted distance. This is required to represent the route in the Flee model. To do this, the cost in hours needs to be represented as kilometres. The route cost is turned into a weighting factor which is multiplied by the Euclidean distance of the route. First, the geometry of the route needs to be calculated. This is done using the tool Calculate Geometry Attributes. This allows for the creation of a new field and the filling of this field in one tool. The length in kilometres is calculated in this way. To get the weighting factor, the speed difference needs to be known: the Euclidean length of the route is divided by the maximum speed that is used earlier in the process. In this case, this is 80 km/h. The length of the route divided by 80 results in the time it takes to travel the route when driving at the maximum speed. Now two time measurements are known for the route. The first, the path cost, as derived from the Cost Path tool and the cost surface, is divided by the time resulting from the maximum speed calculation. The resulting number should be greater than one, and provided the weighting multiplier. This number is multiplied by the Euclidean length of the route, and the weighted distance is the result. The resulting formula is posed in Equation 4.

$$Weighted\ Distance = \frac{Route\ Cost}{\left(\frac{Route\ Length}{Max\ Speed}\right)} * Route\ Length$$

Equation 4: Weighted distance formula.

The implementation of the routes in Flee is done by exporting the weighted distances per route, per season as a .csv file, called routes.csv. This file is then used to replace the routes.csv file already

present in the Flee files. When the model is then run, it uses all the same files as the original Flee model, except for the routes.

3.5 Calibration, verification and validation methods

After creation of the new routes, and the initial running of the adapted model, it is checked if the model works to expectation, and the results are tested. To do this, several steps have to be taken. These steps represent an iterative process, which is visualized in Figure 10.

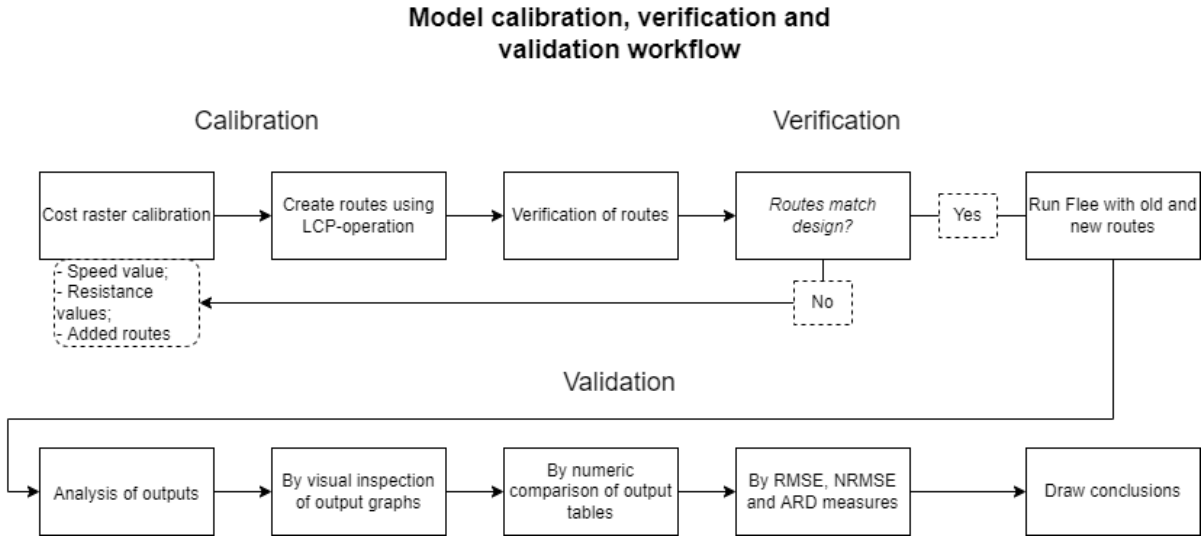

Figure 10: Calibration, verification and validation workflow overview

The first step is calibration. Calibration involves fine-tuning the model to a particular context (Crooks & Heppenstall, 2011). This is done by tuning the parameters of the model so that the model's output matches real-world data, increasing the model's fit to the real-world system. Calibration is an iterative process, changing parameters with until a satisfactory result is obtained (Castle & Crooks, 2006). Once again, this step does not pertain to Flee default parameters, only to cost raster values and the creation of routes. This is done by changing the maximum speed value and the speed multiplier values. While this usually is an iterative process, in this study only one iteration of calibration could be performed due to time constraints.

The next steps are the verification and validation of the model. According to Crooks & Heppenstall (2011), these terms are defined as follows:

"Verification is the process of making sure that an implemented model matches its design. Validation is the process of making sure that an implemented model matches the real-world."

The first of these, verification, pertains to the inner validity of the model (Castle & Crooks, 2006). Verifying the model means checking if the model works as intended. Initially the routes are plotted using the cost rasters that are created using certain speed multiplier and speed variables. It is then checked if the routes are realistic, and follow expected lines. For example, the routes are expected to follow paved routes if available. This check is done by visually inspecting the lines that the routes follow, using satellite imagery, and by matching the new or changed routes to knowledge of local travel patterns from the Ministry of Defence (B. Ooink, personal communication, January 2022). Furthermore, the routes are tested using the Google Maps route planner. The travel times and tracks of several routes are compared to routes plotted between the same start and end locations in Google Maps. However, this method cannot be applied to all routes, as Google Maps does not allow route planning on off-road routes. Therefore, only routes based on road connections can be tested.

The final step, validation, is performed after Flee is run with the calibrated routes data. The goal of the this step is to test if the output is representative of the real-world system. This step requires comparison of the model's results, which are comprised of refugee numbers in camps, to historic refugee data, which is collected by the UNHCR (2021). The result of this step is not binary – the model is not valid or

not-valid. In the case of this study, the most important factor to be measured is if the model has improved by applying the new routes to Flee. This is done using three measures. The first measure is the Root Mean Square Error, or RMSE. This is a measure commonly used to quantify model performance (Chai & Draxler, 2014). As the name suggests, the RMSE is the square root of the average squared errors between the simulated, or projected, values and the observed values. This allows for the comparison of average errors, regardless of the errors being negative or positive. The RMSE formula is found in Equation 5.

$$RMSE = \sqrt{\frac{1}{n}\sum_{i=1}^{n} e_i^2}$$

Equation 5: Root Mean Square Error calculation. Source: Chai & Draxler, 2014.

In the formula, e represents the model error, or the difference between the observed and the simulated value, at iteration i. Lastly, n represent the total number of values (Chai & Draxler, 2014) (Equation 5). The unit of the RMSE output is dependent on the input data. In this case, that means the error given by the RMSE represents refugees. To be more precise: the average squared difference between the simulated amount of refugees and the observed amount for one whole model run.

To allow for comparison between the errors of the camps, the Normalized Root Mean Square Error, or NRMSE, is calculated. This normalization is done by dividing the average RMSE values per camp by the maximum amount of refugees that stay in the camp during the simulation. The result is a value between 0 and 1 for each category.

The third measure is the Averaged Relative Difference, or ARD. This measure is developed by the Flee-team to determine the accuracy of their simulations (Suleimenova et al., 2017). This validation method can be performed using the FabFlee and FabSim add-ons for Flee. These packages provide an environment that facilitates automatic construction, execution and testing of models, as well as validation and visualization tools.

The mean score indicates the averaged relative difference between the camp arrival numbers in the simulation versus those observed by UNHCR. The average is performed across several simulations in what is called an ensemble. In this study, the ARD is calculated for two ensembles of ten simulations each. One ensemble representing Flee runs with the original route files, the other representing the runs with the new route files. The ARD is found in Equation 6.

$$Averaged\ Relative\ Difference = \frac{\Sigma_{x \in s}(|n_{sim,x,t} - n_{data,x,t}|)}{N_{data,all}}$$

Equation 6: Formula for the averaged relative difference. Source: Suleimenova et al., 2017.

The number of refugees found in each camp x of the set of all camps s at time t is given by $n_{sim,x,t}$ based on the simulation projections, and by $n_{data,x,t}$ based on the observed UNHCR data. The total number of refugees reported in the UNHCR-data is given by $N_{data,all}$ (Suleimenova et al., 2017) (Equation 6). If the result of the value is 1.0, this indicates that 50% of the simulation is wrong. An output of 0.0 means that the simulation is completely correct. In this method, the total number of refugees in camps from the simulation is compared to the total number of refugees in camps as observed by the UNHCR.

To further analyse the results, more in depth-inspections of the data are performed. This is done by comparing the graphs and validation results for not only the whole simulation, but spatially and temporally as well. Inspection the results of individual camps and individual seasons provides information on the inner working of the Flee model, and the effects of the adapted routes thereon.

3.6 Mali case study

3.6.1 Study area

The study area for this case study is Mali (Figure 11). Mali is a West-African country with roughly 20 million inhabitants. The capital of Mali, Bamako, is located in the southern half of the country. The northern half of Mali is situated in the Sahara (Bencherif et al., 2020). The southern half is situated in the Sahel region. Besides the Sahara and the Sahel, the primary geographic feature of Mali is the Niger river. Most of Mali's population is dependent on and lives near this river. It enters the country in the south-east and leaves in the south-west. In the centre of the country, roughly on the border of the Sahara and the Sahel, the Niger branches out into an inner delta (Hughes & Hughes J.S., 1992, pp. 191 - 199; Pavelic et al., 2012).

Mali is chosen for this case study as it has been home to internal conflict since 2012 (Shaw, 2013). January 2012 saw the beginning of the conflict, as Tuareg insurgents in northern Mali proclaimed the Republic of Azawad as an independent state from the central Malian government in Bamako. The aim was to form a sovereign state out of the provinces of Timbuktu, Kidal and Gao. The insurgency, originally led by the Tuareg National Movement for the Liberation of Azawad (MNLA), was quickly taken over by Ansar Dine, an Islamist Tuareg group, with the aid of the Maghreb branch of Al-Qaeda (AQIM), after a skirmish between the two groups in the battle of Gao (Shaw, 2013). January 2012 saw a coup d'état, after weeks of protest. The coup was a result of discontent in the military as they found that government support in the fight against the rebels was lacking. In the power struggle, the Tuaregs gained control over Gao and Timbuktu.

One year into the conflict, the French armed forced intervened. Secular Tuareg groups joined forces with the French against the jihadist insurgents. The French offensive saw jihadists driven out of most of northern Mali, but pockets of resistance remained (Bencherif et al., 2020). The conflict has spread towards central and southern Mali as well, where bombings and killings have become the mainstay of the conflict. Furthermore, the conflict has spread across the Sahel region, instilling other conflicts and displacing people outside of Mali as well (D'errico et al., 2021). To counter this spread, the French integrated efforts across the Sahel region into the counter-terror operation Barkhane.

The conflict has led to large numbers of people being displaced (R4Sahel, n.d.; UNHCR, 2021). In the early stages of the conflict, the governments of Niger and Burkina Faso closed their border to the Malian refugees. The total closures were lifted, but travel restrictions on the Mali – Niger border remained, and meant that refugees could only cross the border on foot (Groen, 2016). Currently, some forty-eight thousand refugees have fled Mali, and some four-hundred thousand people are internally displaced (The World Bank, 2021; UNHCR, 2021). These numbers are currently at their highest since the beginning of the conflict in 2012, and are still increasing. As the conflict is mainly taking place in the north and centre of Mali, most refugees are displaced from here as well. Mainly Gao, Timbuktu, Ménaka, Mopti and Kayes have seen large numbers of people flee (Migrants Refugees, 2020; UNHCR, n.d.).

To include all refugee camps relevant to this study, a buffer of three-hundred kilometres is used for the collection of data and the creation of the cost raster. This allows for the plotting of routes to refugee camps outside of Mali (Figure 11).

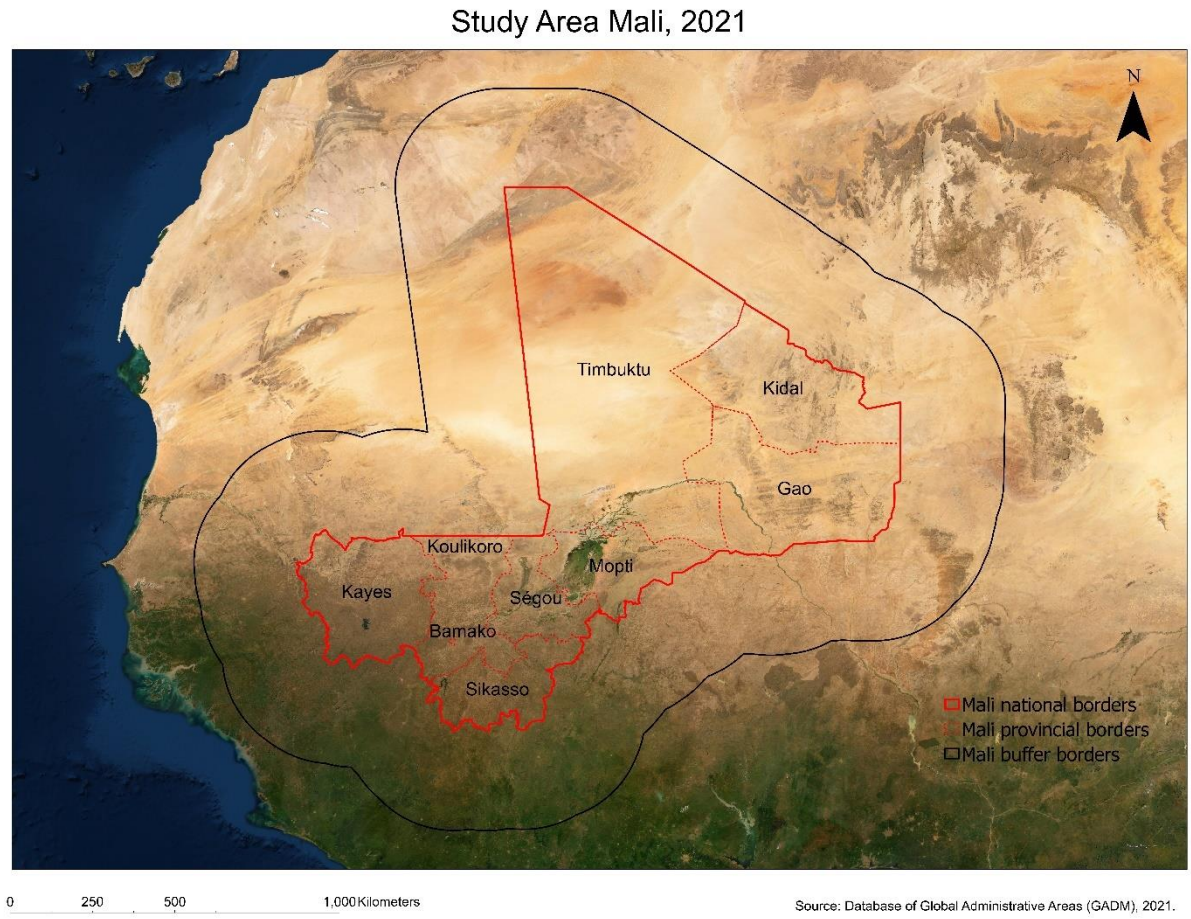

Figure 11: Mali Study Area.

3.6.2. Flee Operationalization

The implementation of Flee for the Mali case study specifically, is explained using six phases defined by Suleimenova et al. (2017).

The first phase marks the selection of a country as study area, and a time period of a specific conflict which resulted in large scale forced migration. For this study, the country is Mali, and the conflict is the internal conflict which started in 2012. The simulation period is 300 days, from the 29th of February, 2012, when the first camp registrations are recorded by the UNHCR, until the 25th of December, 2012, when most refugees had been registered in camps. This period is also used in the simulation performed by Suleimenova et al. (2017), allowing for comparison of results.

The second phase is the acquisition of relevant data to the conflict. The data needed for this phase are conflict, refugee and roads data, which are found on the Armed Conflict Location & Event Data Project (ACLED, 2021), UNHCR (2021) and Bing Maps databases respectively. ACLED data are used for the locations of battles and armed clashes that have taken place within the duration of the conflict. The UNHCR database provides data on refugee numbers during the conflict, as well as camp locations and capacities. Bing Maps is used to obtain the locations of major settlements and routing information between the various camps, conflict zones and other settlements (Suleimenova et al., 2017). The total of settlements, camps, road connections and conflict locations is used to construct the network graph. This graph represents the network in which the agents operate. In this step, two sets of route data are used: the original data, derived from Bing Maps, and the data derived from the Cost Raster and Least-Cost Path methods.

The third phase constitutes the construction of the model with the usage of the aforementioned data. This includes the setting of parameters based on made assumptions (section 3.2).

The locations used in the location graph for the Mali 2012 simulation. These locations form the start points and destinations for agent travel, as well as route nodes. The locations are displayed in Table 4.

Table 4: Locations used for route plotting.

Location name	**Location type**	**Location name**	**Location type**
Abala	*Refugee camp*	Léré	*Conflict zone*
Ansongo	*Conflict zone*	Mangaize	*Refugee camp*
Bamako	*Conflict zone*	Ménaka	*Conflict zone*
Bobo-Dioulasso	*Refugee camp*	Mentao	*Refugee camp*
Bourem	*Conflict zone*	Mopti	*Town*
Diré	*Conflict zone*	Niafunké	*Conflict zone*
Douentza	*Conflict zone*	Niamey	*Refugee camp*
Fassala-Mbera	*Refugee camp*	Ségou	*Town*
Gao	*Conflict zone*	Tabareybarey	*Refugee camp*
Goundam	*Town*	Ténenkou	*Conflict zone*
Kidal	*Conflict zone*	Timbuktu	*Conflict zone*
Konna	*Town*		

The locations used in the plotting of the adapted and new routes are the same as the locations in Table 4. The connections between these locations are determined in two ways. The largest amount of connections is already determined for the initial Flee run for Mali 2012. These connections are based on the presence of a direct road connection in Bing maps, and are used again in the adapted run. The connections are taken from the GitHub Flee files. However, the weighted distances for these routes are recalculated through the method described in section 3.4. The second way in which the connections are determined applies to the newly created routes. These connections are based on estimations of logical routes, that were deemed missing in the original location graph (section 3.2). These estimations were done in consultation with an expert from the Dutch Ministry of Defence, who is knowledgeable on the local travel patterns of refugees (B. Ooink, personal communication, January 2022). The route creation results in four different distances for each route, one distance for each season. The location graph consists of 44 routes. These are plotted four times each, one per season. The result is 176 routes, which differ in weighted distance per season. The resulting location graph, including new routes, is displayed in Figure 12.

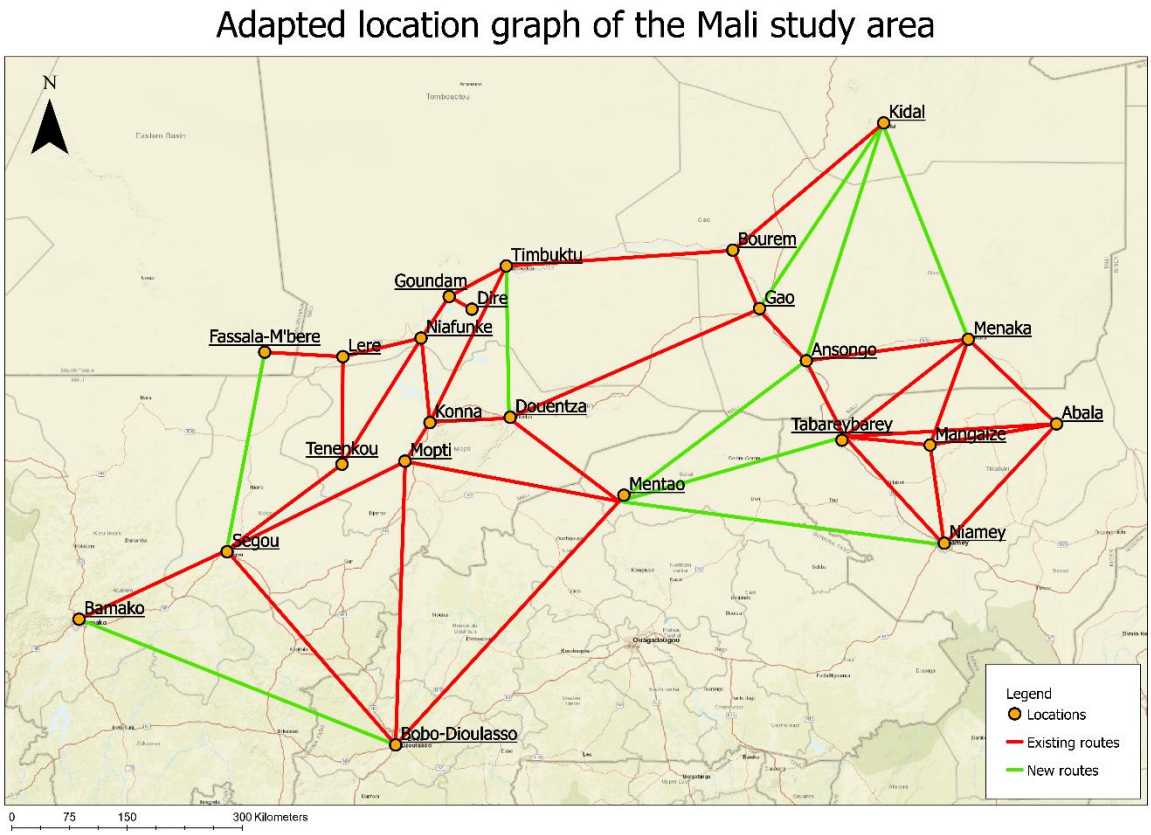

Figure 12: Adapted location graph.

From the locations described in Table 4, some areas are set in the Flee model as conflict zones. The model allows for assigning conflict location during the model run, at a certain timestep. These emergent conflicts change the way the agents behave in the model, and affect the routes and destinations that the agents take. The data for these conflicts is sourced from the ACLED Database (Suleimenova et al., 2017). The conflict zones, and the timesteps at which they emerge or disappear, are displayed in Table 5.

Table 5: Conflict zone emergence days.

Location name	**Conflict zone emergence day**	**Location name**	**Conflict zone emergence day**
Abala	-	Léré	*273*
Ansongo	*30*	Mangaize	-
Bamako	*163*	Ménaka	*2*
Bobo-Dioulasso	-	Mentao	-
Bourem	*30*	Mopti	-
Diré	*13*	Niafunké	*1*
Douentza	*185*	Niamey	-
Fassala-Mbera	-	Ségou	-
Gao	*23*	Tabareybarey	-
Goundam	-	Ténenkou	*3*
Kidal	*1*	Timbuktu	*1*
Konna	-		

Once the model setting is constructed and the parameters are set, the fourth phase begins, which consists of refining the model. By default, the total number of refugees is found by taken the historic total aggregated number of refugees in camps, as measured by the UNHCR. Furthermore, each timestep, a number of refugees is inserted into the simulation based on the daily increase in the total refugee registration count from the UNHCR data. The refugees are inserted in one of the conflict

locations, based on the population of that location (Suleimenova et al., 2017). These UNHCR refugee data are visualized in Figure 13.

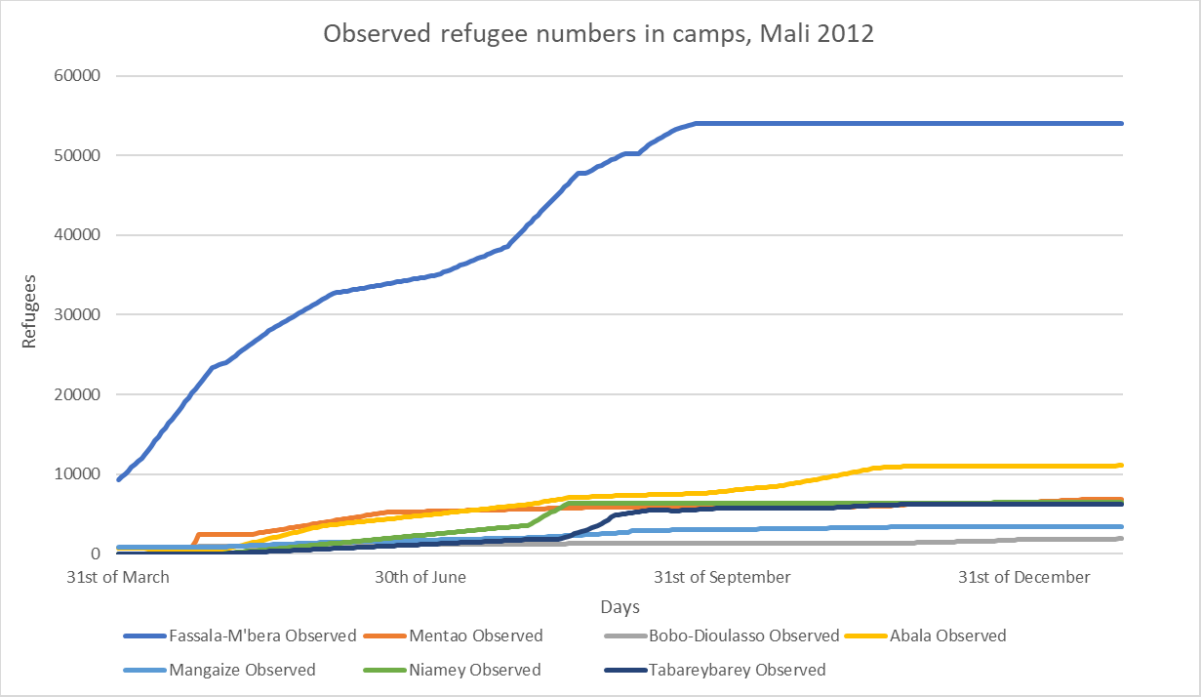

Figure 13: Observed refugee data, Mali 2012. Source: UNHCR, 2021.

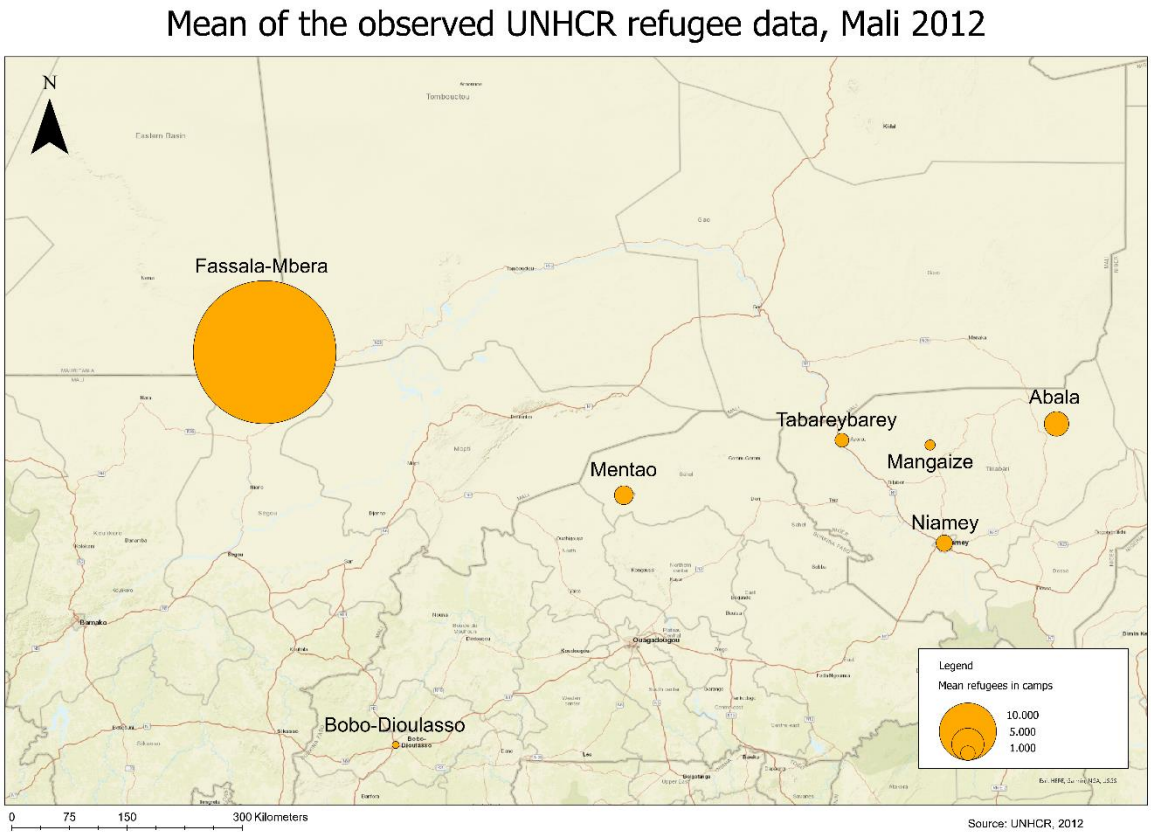

Figure 14: Mean observed refugee numbers over the complete time period. UNHCR, 2012.

The refugee numbers in Mali are not equally distributed, as can be seen from Figure 13. To provide a spatial perspective on this division, the mean of these refugee numbers are displayed as proportional symbols in Figure 14. The camps Fassala-Mbera and Abala account for some 75% of the Malian refugee numbers in 2012. Where the graph lines remain constant towards the end of the time period, the camp capacity has been reached. This can be clearly seen for Fassala-Mbera in Figure 13. Where the graph-line remain constant at the start of the simulation, border closures are in place. This can be seen for the camps Mangaize and Tabareybarey. Another part of phase four consists of adding the border closure data to the model. These closures are displayed in Table 6.

Table 6: Closure data and dates for the Mali case study, 2012.

Name1	Name2	Closure start	Closure start date	Closure end	Closure end date
Mali	*Burkina Faso*	*0*	*29th of February, 2012*	*22*	*22nd of March, 2012*
Mali	*Niger*	*0*	*29th of February, 2012*	*33*	*1st of April, 2012*

Phase five involves the simulation run in Flee. This is used to project the distribution of refugees across the individual camps. In this study, Flee is run a total of twenty times. The first ten times with the original routes data, the second time with the adapted routes data, based on the cost raster.

The final phase involves analysing and validating the results against the full UNHCR refugee numbers. This is described in detail in section 3.7.

In this study, phases two through four are already finished. The Flee files, available on Github (https://github.com/djgroen/flee), include the finished products of these steps. The usage of these files allows for a run of Flee with the default settings. The purpose of this study requires only that the routes data from these files are adapted.

3.7 Data

The data used in this study are selected to represent the features of the physical environment that are relevant to a refugee. The data that represent these features are described here. The datasets linked to the NATO-classes are summarized in Table 7, and explained below.

Table 7: Summary of data used in the study.

Type	Feature	Data
Relief	Slope – percentage of incline – non-seasonal feature	JAXA ALOS Global 30m DSM (2021)
Drainage	Presence of open water and wetlands / floodplains – seasonal feature	Sentinel 2 – Indexed satellite images (NDMI / Wetlands in Water (WiW))
Soil	Surface material – loose sand, rocky surfaces and compacted sand/gravel/grassland– partially seasonal feature	Sentinel 2 - Esri Land Cover 2020
Infrastructure	Presence of roads, bridges, ferries or fordable river sections –partially seasonal feature	Open Street Map; Esri Land Cover (2020)

3.7.1 Relief

The *Relief* data class is comprised of the slope feature, or the percentage of incline between different elevations. This feature is derived from the Japanese space agency's ALOS global digital surface model. The newest version, 3.2, is released in January 2021. This DSM has a horizontal resolution of approximately 30 meters, or 1 arcsecond (Google Earth Engine, 2021). From this elevation dataset, the slope is derived in Google Earth Engine (GEE). For the purpose of representing the Earth's terrain, usually a digital terrain model (DTM) instead of a digital surface model (DSM) is used, as a DSM includes the elevation of all objects present on the Earth's surface. In this case however, a DSM is used, as there is no DTM available for Mali with the same level of resolution. Furthermore, the ALOS DSM is the most recent one compared to available DTMs. Inspection of the data has shown that the DSM provides no significant negative effect to the accuracy of the terrain representation. The most significant elevation differences and slopes are limited to the north of Mali, where the is little to no tall vegetation capable of disrupting the data. The slope data were then reclassified into five classes. The slope data used in this study is assumed to not change seasonally.

3.7.2 Drainage

The datasets that are part of the *Drainage* data class are 'open water' and 'wetlands' or 'floodplains'. To create these data, multi-spectral images from ESA Copernicus' Sentinel 2 1C mission were used. As the presence of water in Mali is prone to seasonal change, using a single, predefined dataset that delineates water bodies is not suitable for this study (Andersson et al., 2017; Casse et al., 2015). Therefore, a different method is used. Sentinel 2 multispectral images are classified using the NDWI, yielding a dataset with values between 1 and -1 (Equation 1, section 3.3).

Copernicus' Sentinel 2 data are useful for this study due to several reasons. Firstly, the Sentinel 2 mission retrieves high spatial-resolution images in several different bands. These bands include visible light and near-infrared light, which makes the data suitable for NDWI calculations. Secondly, the temporal resolution of the data is high. The revisit time of the Sentinel 2 satellites is approximately five days. This allows for comparing the signal over time and detecting seasonal change accurately. To do this, the data is first classified into four seasons. The start and end dates of these seasons can be found in Table 8.

Table 8: Dates used for seasonal reclassification.

Dates used for seasonal reclassification of Sentinel data		
Seasons	*Start date*	*End data*
Season 1	1st of January	31st of March
Season 2	1st of April	30th of June
Season 3	1st of July	31st of September
Season 4	1st of October	31st of December

The dry season marks the period where the Niger river is at its largest. This is caused by the water upstream arriving with a delay downstream. This period falls generally between October and March, so from seasons 1 through 4. The wet season ranges roughly from April through September, in seasons 2 and 3. In this period, the water volume in the Niger is at its lowest. This reclassification of the Sentinel data is applied to all years between 2015 and 2021. The same seasons from each year are combined. On this combination, the median is calculated. From this calculation, cloudy images are excluded to yield a higher accuracy. For Northern Mali, a 0-percent cloud cover tolerance could be set, removing all images with clouds and thus resulting in the highest accuracy. However, the inclusion of the buffer around Mali meant that some of the data represent tropical areas, where cloud cover is a much more common occurrence. This means that a 0-percent cloud cover tolerance results in data gaps, for areas where there are no cloudless images available. Therefore, a 15-percent tolerance is applied to reduce the amount of data gaps to an insignificant amount and location. This results in a lower accuracy signal.

The result is a dataset for each season that depicts the median signal retrieved by Sentinel 2 over the span of six years, yielding a cloudless dataset that depicts for each cell the most likely signal. On this seasonal, multi-year median, the NDWI is calculated. In this study, the NDWI data are used to classify the region into a binary dataset, depicting open water and non-open water.

Another challenge is the classification of wetland surfaces. These are classified using the *Water in Wetlands* method, published by Lefebvre et al. (2019) (Equation 2, section 3.3). Before applying this method, the Sentinel 2 signal does need to be divided by ten-thousand, to transform the raw signal into reflectance values (*GIS Ag Maps - Sentinel-2 Surface Reflectance Tutorial*, n.d.).

To create a coherent dataset, first the NDWI values are reclassified: positive values indicate the presence of open water (value = 1), negative or 0-values indicate land (value = 0). The resulting four reclassified datasets of the NDWI method are then merged with the four dataset of the WiW method, resulting in one dataset that delineates all areas where water has been for the duration of at least one seasonal median. In other words, it delineates the areas that have the possibility of containing water or wetlands throughout the year, which would make those areas impassable. In the model, these areas are all assigned the value 0.5, which is the speed multiplier value of dry floodplains (see section 3.8.1). However, a conditional statement is added that if a cell from this dataset is overlapped by a cell from one of the seasonal datasets of either the NDWI or the WiW, the cell becomes impassable, by assigning the speed multiplier value 0. The result is a dynamic way to differentiate between water and wetlands, which are impassable, on one hand, and dried-up floodplains on the other hand.

3.7.3 Soil

The data class *Soil*, from the NATO classification, pertains in this case study mostly to surface material, as most soil specifications, beside moisture level, are not relevant to refugee flight behaviour. The surface of Mali is reduced to three classes, besides open water and wetlands, which are explained in different sections. These three classes are *compacted sand/gravel/grassland, loose sand* and *rocky areas*. The first class serves as a 'rest' class, which is used to delineate all surfaces besides *loose sand* and *rocky areas*. This includes for example all vegetated areas. As no distinction is made between vegetation presence, type or density, this choice is made. Furthermore, from personal communication the *rocky areas* and *loose sand* features were deemed the most common in Mali and the most influential to vehicular travel (B. Ooink, personal communication, September 2021).

To delineate these classes in the terrain, two methods are used. The first method is to reclassify the Esri Land Cover 2020 dataset. This dataset consists of a raster with a 10-meter resolution, in which areas are divided into 10 classes, derived from Sentinel 2 data. This dataset is used for each season,

as it is assumed that the used land cover features do not change seasonally. From this dataset, *loose sand* and *compacted sand/gravel/grassland* are derived. Through visual inspection, loose sand is assumed to form the 'bare areas' class in the Esri dataset. All other classes in the dataset are reclassified to form the *compacted sand/gravel/grassland* class. The data are then aggregated to a 30-meter resolution dataset, to match the other datasets used in the study.

The second method is used to classify *rocky areas.* The *rocky areas* class is derived through a random forest supervised classification of Sentinel 2 images (section 3.3). The classified Sentinel 2 images were reclassified into a binary dataset, delineating 'rocky areas' and 'non-rocky areas'.

3.7.4 Infrastructure

The data class *Infrastructure* consists of several roads features. The *roads* dataset is derived from Open Street Map (OSM), and open-source infrastructure data source that is frequently updated. The OSM database is accessed by using the QGIS plug-in QuickOSM. Open Street Map offers several classes that represents roads and river crossings, which is ideal for the dynamic situation of Mali's rivers. The roads dataset is split into five classes that are suitable for vehicular traffic: primary roads, secondary roads, tertiary roads, residential roads and unclassified roads. The first two classes consist of highways, with the highest degree of accessibility, meant as national connections. Tertiary roads are smaller, regional roads. Residential roads are roads within urban areas, and unclassified roads are local, sometimes unofficial roads.

Furthermore, in the OSM data several properties in the roads dataset are included that are important to simulating the situation in Mali. This is the case due to the significant changes in waterflows that occur periodically in Mali. Some routes of travel are not viable in one season, while they are in another season, due to the swelling and shrinking of the rivers. These properties include the presence of bridges, ferries and fordable areas. It is assumed that vehicles used by refugees do not have the capability to traverse open water, and are therefore reliant on these crossings. To select bridges, road sections where the property *bridges* equals *T* (for 'True'), are stored in a separate file. The same is done for the property *ford*, which indicates a fordable area. Next, to select ferries, the point dataset 'Ferry terminals' is taken. To include ferries in the road network, vertices were manually drawn between the ferry terminals and the nearest road. Some 40 ferry connections exist in Mali according to OSM, with an additional 26 in the buffer area. To ensure the connection would transfer correctly to raster data, the river crossings were buffered using the *Buffer* function, with a diameter of 90 meters, or roughly three cells. All data are then converted to raster using the ArcGIS Pro tool *Feature to Raster* to allow for the inclusion of the data in the model.

In the periods when the Niger river is generally at its peak volume, in seasons one and four, fords are made inaccessible in the model. The opposite is true for ferries, which are not accessible in seasons two and three, when the river is reduced in size and volume. Bridges are available throughout the seasons. This results in the need to take different routes in different seasons, as some river crossing become inaccessible.

3.8 Speed multiplier values

3.8.1 Surface speed multiplier values

The speed multiplier values for different surface materials are determined using literature sources. As no single source is found that described the needed values completely, the values used for this study are a combination of several studies The values for roads and open water are not determined from literature. It is assumed that maximum speed can be obtained on roads, as these are usually the paths of least resistance for vehicles. This maximum speed value is already adapted to the quality of roads in the study area. Water is given the value 0, representing an impassable object. In the table, wet and dry seasons are given different values, as some terrain surfaces might be affected by this fluctuation.

The first source is a document that describes a standard method for ground vehicle mobility, used by NATO (Baylot et al., 2005). This NATO Reference Mobility Model (NRMM) in itself could not be used, as it requires information too specific for this study, such as vehicle details. In this report however, a 'roughness' factor is assigned to several surface materials. The roughness factor in this report is a comparative value to several different climate regions. This roughness factor represents resistance and

is therefore converted on a 1:1 ratio to a speed multiplier value. The values in Table 9 are not the actual values found in Baylot et al. (2005), but are standardized to values between 0 and 1, by dividing the values by the maximum value. The values are then inverted to match with the other values, where 0 represents no movement possible and 1 represents no slowdown.

Table 9: Speed multiplier values as described in Baylot et al. (2005).

Feature	Original speed multiplier value (Baylot et al., 2005)	Standardized speed multiplier value	Standardized inverted speed multiplier value
Compacted sand/gravel/grassland	*0.6*	*0.3*	*0.7*
Loose sand	*0.3*	*0.15*	*0.85*
Rocky surface	*1.8*	*1*	*0*
Wetlands	*1.8*	*1*	*0 (described as mangrove)*
Floodplain	*0.3*	*0.15*	*0.85 (described as wetland)*

In Table 9, the speed multiplier values from Baylot et al. (2005) are described. Loose sand is the least resistant surface according to the source, along with wetlands. As the source describes wetlands for deserts, the speed multiplier value is low (0.3). This is probably due to desert wetlands being comparatively trafficable in comparison to wetter climate areas. Therefore, this value is assumed to represent closest a floodplain in the dry season. Baylot et al. attribute the lowest speed multiplier value to mangroves and rocky surfaces. Mangroves are assumed to represent bogs or swamps in the case of Mali. All these surface types can be classified as wetlands, which is the term that is used from here on.

The second source used for the determination of the speed multiplier values is an analysis of historical cross-country mobility projection in Germany by F. Malm (2019). Included in this document is a map which uses a Likert classification to rank the 'trafficability' of different surfaces. Once again, this trafficability value is converted on a 1:1 ratio to a speed multiplier value. In this rating a distinction is present for wet and dry conditions as well. The values have been made numerical to allow for comparison. The rating is described in Table 10.

Table 10: Speed multiplier values as described in Malm, (2019).

Feature	Speed multiplier value scale (Malm, 2019)	
	Dry season	*Wet season*
Compacted sand/gravel/grassland	*0.8*	*0.6*
Loose sand	*0.6*	*0.8*
Rocky surface	*NA*	*NA*
Wetlands	*0*	*0*
Floodplain	*0.2*	*0*

The values described in Table 10 are somewhat different to the desert speed multiplier values of Baylot et al. (2005), as the values in Malm (2019) describe an area in Belarus. Loose sand for example probably does not describe the same material in both sources. However, the hierarchy of the values is roughly the same.

The third and final source is written by M. Rybanský (2003). Rybanský has written multiple paper on the effect of geographic features on cross-country movement for the Brno Military Academy in the Czech Republic (Hubáček & Rybansky, 2013; Rybanský, 2003; Rybansky et al., 2015). The approach to determining the resistance of surfaces in his paper is more simplistic. Features are divided in one of three groups: *GO, SLOW GO or NO GO.* These groups are represented in the raster by the speed multiplier values 1, 0.5 and 0 respectively (Rybanský, 2003). These values are assigned to the pertinent surfaces in Table 11.

Table 11: Speed multiplier values as described in Rybanský (2003).

Feature	Speed multiplier value (Rybanský, 2003)
Compacted sand/gravel/grassland	*1*
Loose sand	*0.5*
Rocky surface	*0*
Wetlands	*0*
Floodplain	*0.5*

In their description, several different terms are used. ‘Clayish soil during wet weather’, belonging to the *SLOW GO* group, is interpreted as a floodplain in wet weather. ‘Powdered soil during dry weather’, belonging to the same group, is interpreted as loose sand.

To summarize the values derived from these sources, an overview can be found in Table 12.

Table 12: Speed multiplier values summarized.

Feature	**Baylot et al., 2005**		**Malm, 2019**		**Rybanský, 2003**	
	Dry season	*Wet season*	*Dry season*	*Wet season*	*Dry season*	*Wet season*
Compacted sand/gravel/grassland	*0.7*	*0.7*	*0.8*	*0.6*	*1*	*1*
Loose sand	*0.85*	*0.85*	*0.6*	*0.8*	*0.5*	*0.5*
Rocky surface	*0*	*0*	*NA*	*NA*	*0*	*0*
Wetlands	*0*	*0*	*0*	*0*	*0*	*0*
Floodplain	*0.85*	*0.85*	*0.2*	*0*	*0.5*	*0.5*

The mean is calculated on the values listed in Table 12, and the results are displayed in Table 13. The value for floodplains in the wet season amounts to 0.45 according to the literature. However, studies have shown that wetlands are only accessible for high-end tracked vehicles (Guo & Lu, 2009). Therefore, it is assumed in this study that these surfaces are not passable for refugees travelling in ordinary, wheeled vehicles. The class floodplains used in literature is merged with the class wetlands, as they both represent an impassable surface when wet. The speed multiplier value for these surfaces is therefore not bound to the season, but to the measured amount of moisture in or on top of the soil. When wet, they are treated as impassable. When dry, they are treated as reducing trafficability to 50%, which is derived from the mentioned literature. This is possible due to the dynamic nature of the data that represent these surfaces, and is further explained in the Data section (section 3.7.2).

Table 13: Averaged speed multiplier values.

Feature	**Speed multiplier values**	
	Dry season	**Wet season**
Roads	*see Table 9*	*see Table 9*
Compacted sand/gravel/grassland	*0.8*	*0.8*
Loose sand	*0.7*	*0.7*
Rocky surface	*0*	*0*
Wetlands	*0.5 (when dry)*	*0 (when wet)*
Water	*0*	*0*

However, testing has shown that these values are still high, and might provide a distorted image of reality, in comparison to the roads speed multipliers. Besides the physical resistance of surfaces, there are several components that play a role in the actual accessibility of surfaces as well. First, off-road surfaces are less accessible not only due to the soil structure, but also due to land-cover objects. For example, although vegetation is not taken into account directly into this study, it still plays a role in the accessibility of surfaces. Roads, especially non-paved roads, are generally defined by their lack of obstacles such as vegetation and rocks, which makes them accessible and often the chosen route of travel. Areas outside of roads, paths or trails generally have some degree of obstacles, be it vegetation, rocks or uneven surfaces. Second, there is a mental factor at play. If provided with a choice, people most likely pick a path or trail over an area devoid of visible routes, even it might take more time. Furthermore, there is a factor of not knowing how much longer it takes to drive along a road instead of going off-road.

These factors are difficult to quantify. It is assessed that the extra resistance factors amount to a further decrease of roughly 50% of the speed multiplier values. The results of this are displayed in Table 14.

Table 14: Final speed multiplier values.

Feature	**Speed multiplier values**	
	Dry season	**Wet season**
Roads	*see Table XX*	*see Table 9*
Compacted sand/gravel/grassland	*0.4*	*0.4*
Loose sand	*0.3*	*0.3*
Rocky surface	*0*	*0*
Wetlands	*0.5 (when dry)*	*0 (when wet)*
Water	*0*	*0*

The roads data speed multiplier values are split up into several classes (Table 15). This is done to represent the different quality of different road types. The values range from 1 to 0.8. The lower value, 0.8, is set to not go below the least resistant non-road surface, which is compacted sand/gravel/grassland. With the exception of river crossings, all road speed multiplier are either equal to or higher than 0.8. The first class, primary roads, represents national highways. This class is set to 1, representing that these roads allow for the maximum speed to be obtained (Ramm, 2021). Secondary roads represent regional roads. Visual inspection of the dataset shows that some of these roads are paved, but are of lesser quality in comparison to the primary roads. Therefore, the speed multiplier value of this layer is slightly increased. Tertiary and residential roads are assigned the same value. These local or regional roads are either of lesser quality or reduce maximum speed through traffic regulations. The value is therefore 0.9 (Ramm, 2021). Unclassified roads can be any road or path that cannot be assigned to a specific class. These roads allow not much faster travel than some roadless areas. The difference is therefore only 0.05 to compacted sand/gravel/grassland (Table 15).

Table 15: Road speed multiplier values.

Road class	**Speed multiplier values**
Primary roads	1
Secondary roads	0.95
Tertiary roads	0.90
Residential roads	0.90
Unclassified roads	0.85
Bridges	0.50
Fords	0.20
Ferries	0.10

The river crossing classes are classified separately. Of the three classes, ‘bridges’ allows for the faster travel. Some bridges might be more narrow than the connecting roads, and therefore demand a significant slowdown. Fords slow down more, to represent having to drive carefully through an inundated area, reducing the speed by 80% in this case. Ferries have the lowest speed multiplier, representing waiting time for the ferry to arrive, and slow transport across the waterbody.

3.8.2 Slope speed multiplier values

The speed multiplier values for different slope angles are derived from literature as well. The method described by Shoop et al., (2005) is a simplified classification derived from the NRMM method (Baylot et al., 2005). It defines five classes of slopes, each of which gets assigned a speed multiplier value (Shoop et al., 2005; Suvinen, n.d.). The maximum slope in this method is 30%. Slopes above this angle are classified as no go terrain. However, the values described by Shoop et al. are meant to represent military vehicles, which are often suited for rough terrain and equipped with four-wheel drive capabilities. Therefore, the values for this case study are adjusted to represent the wide range of vehicles that might be used by refugees. The speed multiplier value is increased to represent this difference in vehicle power and capabilities. The classes, values and slowdown factors are listed in Table 16. The values that are used in the raster are listed under the *adjusted speed multiplier factor.*

Table 16: Slope speed multiplier values, derived from Shoop et al. (2005).

Slope class (%)	Speed reduction percentage	Speed multiplier value	Adjusted speed multiplier value
0 – 5	*0%*	*1*	*1*
5 – 15	*10%*	*0.9*	*0.8*
15 – 25	*20%*	*0.8*	*0.6*
25 – 30	*30%*	*0.7*	*0.4*
>30	*NoGo / 100%*	*0*	*0*

4. Results and Discussion

4.1 Route creation results

In Figure 15, the plotted routes for season 1 are showcased. The way some of the routes differ per season can be seen in Figure 16. Here, the season 1 routes are overlayed by the routes plotted for season 3.

Figure 15: Plotted routes with season 1 data.

Figure 16: Difference in plotted routes.

The routes generally follow the major roads, unless large shortcuts are possible, or when road connections or river crossings are lacking. Routes in several cases merge on the same path, as there are major roads present. This can for example be seen near Bobo-Dioulasso (Figure 16). The route from Ségou towards Bobo-Dioulasso includes a detour to meet-up with the highway towards this city. This pattern is expected, as the speed multiplier values for the roads are higher than the off-road speed multiplier values.

The differences in route distances can amount into several hundreds of kilometres, and are induced by the changes in river crossing accessibility. For example, the connection between Mentao and Ansongo is significantly shorter in season one in comparison to season three, due to the accessibility of a ferry crossing just south of Ansongo. This ferry is not available in the wet season due to low water levels in the river (Figure 16). The full changes between the routes are listed in the Table 17 (Appendix 7.1). On the weighted distances of the routes, the percentual differences are calculated between the old and new values (Table 17, Appendix 7.1). As the new routes consist of four values, the average of these values is used. This comparison can only be applied to the connections that already existed in the original location graph. Mainly the weighted distances for the routes between Konna and Niafunké and Konna and Timbuktu have increased, by 397% and 153% respectively. This can be explained by the proximity of Konna to the Niger river and Inner Niger delta. The routes to Konna increase in season two and three, indicating a reliance on ferry crossings for accessibility. The positive relative differences for all other routes have remained below 50%. Relatively the largest negative difference in route weighted distance happens for the Douentza – Mentao route, where the weighted distance decreased by 44%. On average, the routes for season one and four have increased by 17%. In seasons two and three, this difference is nearly twice that, at around 30%. This difference is caused by the absence of ferry crossings in seasons two and three, and the absence of fordable areas in seasons one and four. The amount of ferries exceeds the amount of fordable areas, explaining the larger impact of the absence of ferries on the plotted routes (Table 17, Appendix 7.1).

Several routes are tested for accuracy of travel time, and thus weighted distance, as well as of the plotted paths for the routes. The simulated routes follow largely the same track for each of the tests as the route planner in Google Maps. This indicates that the speed multipliers for off-road travel compared to on-road travel are within proportions, and the hierarchy of resistance is accurate. In other words, it is represented correctly that on-road travel is preferred on a route if this option is available.

The tests for travel time show that on average for the tested routes, the difference in travel time for the routes is ~13% (Table 18, Appendix 7.2). A certain percentage of error is expected in the creation of routes, and the 13% difference seems and acceptable error for the creation of off-road routes. However, this might not represent the actual travel time difference for all simulated routes and the real-world routes, as not all routes can be tested in this way. The comparison does show, that the speed multiplier for roads in combination with the maximum speed value, are roughly 87% accurate. Furthermore, the results in Table 18 (Appendix 7.2) shows that for each of the tested routes, the simulated travel times are lower than the observed travel times. This means that the speed multiplier value and the maximum speed are more optimistic than reality. Thus, in reality, travel takes longer than simulated. Further calibration of these values is required to amend this. The accuracy of off-road routes cannot be validated in the same manner however, and requires field testing to validate. Only the accuracy of the new method for the routes that follow the same paths as the original routes can be tested.

To summarize, the routes do follow the same tracks, which indicates an accurate ratio of speed multipliers between road and non-road values. However, on-road travel speeds are too optimistic. To more accurately represent reality, the maximum speed or the speed multipliers for roads used in the simulation should be reduced. For off-road travel, both the accuracy of the plotted routes, as well as the accuracy of the multipliers and the maximum travel speed remain unknown.

4.2 Flee results

The results of the Flee simulations are described and discussed here. Figure 17 and 18 show the results of both the simulations with the old routes and the simulations with the new routes.

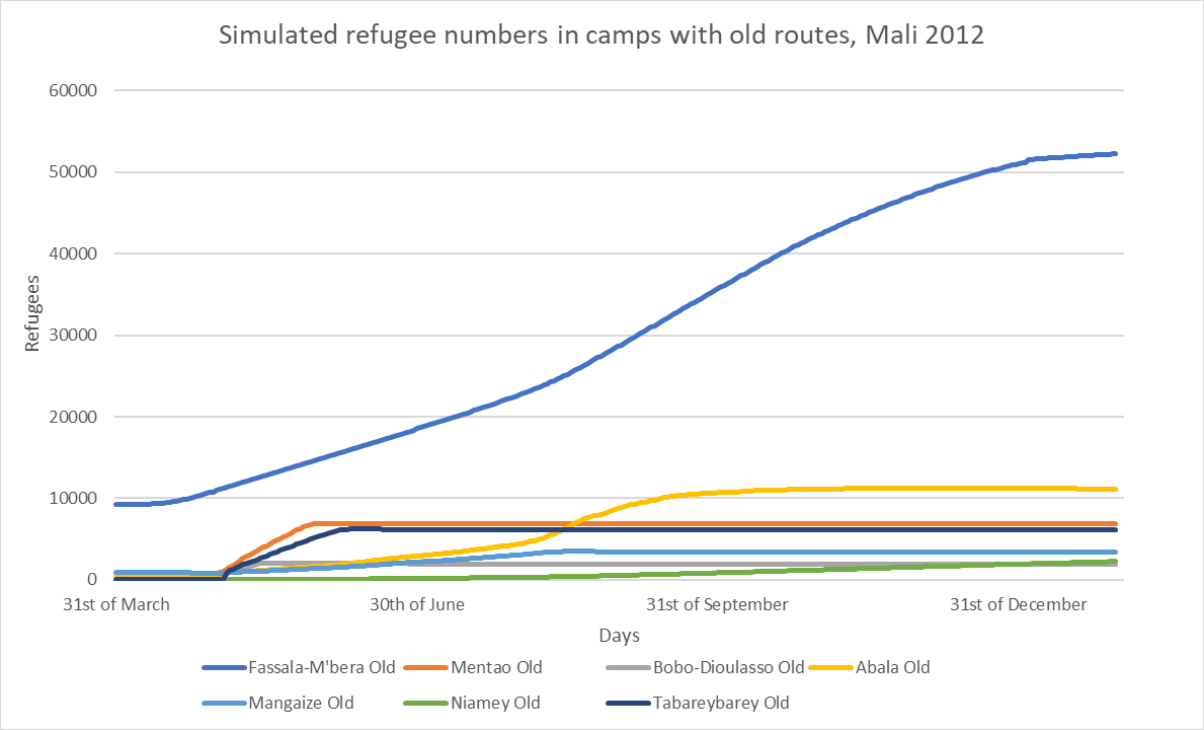

Figure 17: Old routes average refugee numbers per camp.

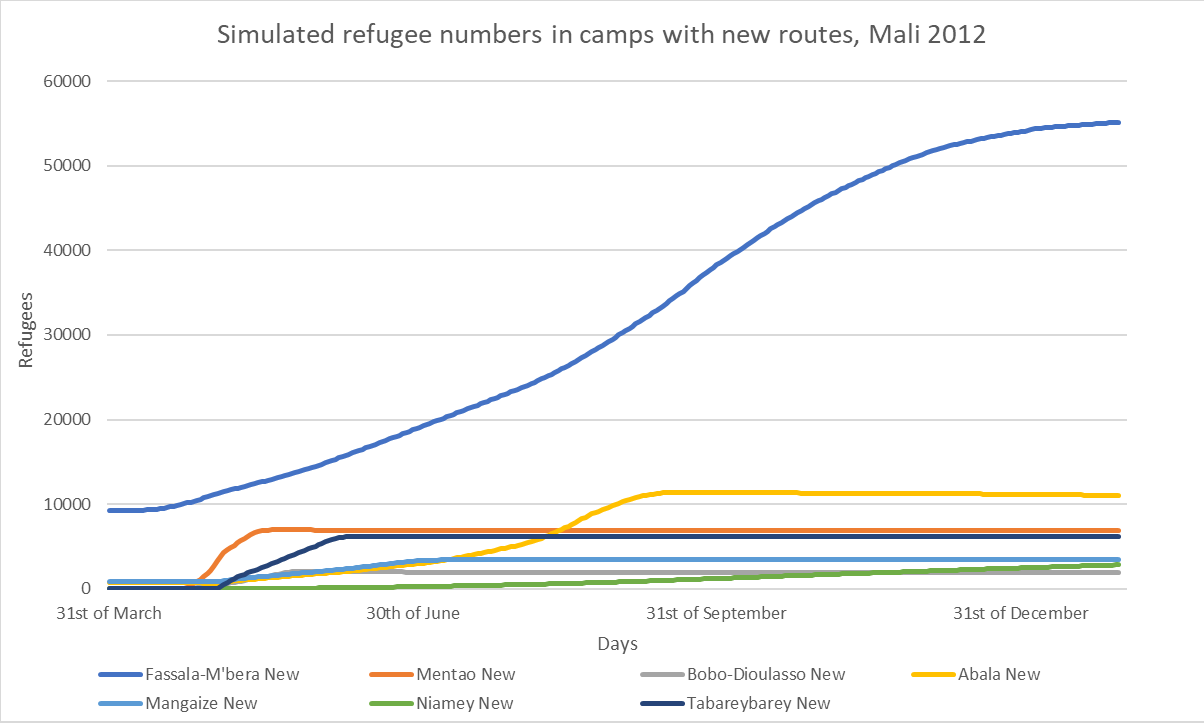

Figure 18: New routes average refugee numbers per camp.

Figure 17 and 18 show that the results of both simulations are comparable to the observed data from the UNHCR (Figure 13 – section 3.6.2). In all cases, the camp Fassala-Mbera has the largest population of refugees. In both simulations, the next largest amount of refugees towards the end of the simulation

can be found in Abala. Abala and Fassala-Mbera still account for some 75% of refugees in the simulation. This can be explained by these camps' proximity to early conflict locations and the high refugee capacity. For Fassala-Mbera, the locations are Niafunké, Ténenkou and Timbuktu. For Abala, these are Timbuktu and Ménaka. After Abala, the next largest camps are Mentao and Tabareybarey. This is what the observed data show as well.

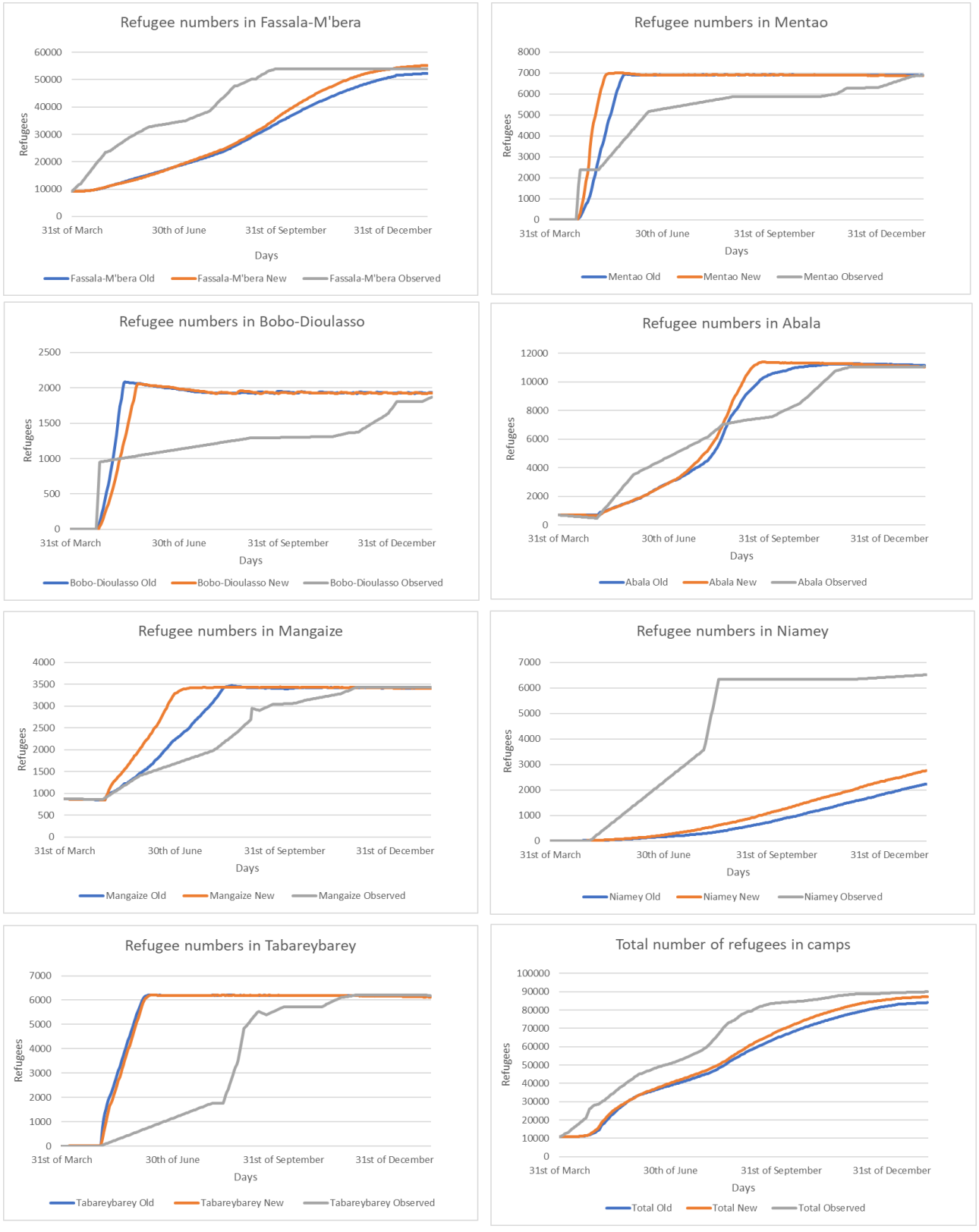

Figure 19: Average refugee arrival numbers per location.

To analyse the differences between camps in more detail, the average refugee numbers over ten runs of the individual camps are plotted in Figure 19. The new routes have caused a difference for all locations, with the exception of Tabareybarey. A difference between the simulations and the observed data is the underestimation of refugees in Niamey, and the overestimation of refugees in the Niger camps of Abala, Mangaize and Tabareybarey (Figure 19). These two trends are most likely related in the following way: Niamey is a capital city, undoubtably known to many across the border in Mali as well. Being a large city, Niamey might have an attractive value that is not taken into account in the model (Suleimenova et al., 2017). A city such as Niamey is often the best supplied in the country, and home to most resources and amenities in the country. Compare this to a refugee camp, and a large city quickly becomes the more desirable option to flee to. In a study performed using Flee, Campos et al. (2019) state that:

"(..) food security influences the likelihood of travelling refugees to depart (..)."

(Campos et al., 2019)

Furthermore, in the beginning of the conflict, the Niger refugee camps were in a poor state. The UNHCR states the following:

"Many of the new arrivals are sleeping in the open and have little access to shelter, clean water, health services and food. (…) people were scattered mainly in villages (…) in the north of the country. Sinegodar, a village in Tillabery district, is hosting more than 5,500 Malians, with only one water outlet for the refugees and the local population."

(UNHCR, 2012)

However, in Flee the opposite of the desire to leave camps in favour of the city is represented. The chance that an agent leaves a camp is 0.1%, resulting in most refugees staying in the first camp they arrive at after crossing the border, unless the camp capacity is reached. In reality, refugees might not be as satisfied in those camps as assumed in the model, especially when food accessibility is low, which is the case for the Niger camps during the study period, according to the UNHCR (2021).

Some refugees in Abala and Mangaize have crossed the border during or before the border closure. This can be seen in the simulation results, where the refugee numbers in the camps remain constant at around 1000 refugees before the opening of the border (Figure 19).

After the reopening of the border, the Mali-Niger border remained subject to limited border restrictions that were still in place after the border opening on day 33 of the simulation, or the 1st of April, 2012. The restrictions meant that refugees could only cross the Mali – Niger border on foot (Groen, 2016). These restrictions remained in place for the duration of the conflict. Such restrictions are not taken into account in the model either. This might further play a role in the overestimation of refugees in the aforementioned Niger camps. Zolberg et al. (1986) state the following:

"The most problematic type of external effect consists of the policies of potential receivers. (..) People cannot leave their country if they have no place to go; and in effect, in a world of generally restrictive controls on entry, the availability of such a place is largely determined by the governmental policy of receiving [countries]."

(Zolberg et al., 1986)

The importance of international policy means that the absence of such international refugee policies in the model is potentially damaging to the accuracy of the results.

Besides the discrepancy that is present between both simulated datasets and the observed data, an increase in this discrepancy after the implementation of the new routes is seen as well. This is mainly notable for Mangaize, where the distance between simulated and observed data has clearly increased. The Mangaize graph in Figure 19 shows that the new simulation does not assign more refugees to Mangaize, but assigns the same amount of refugees earlier to the camp. This can be explained by looking at the distances of the routes towards Mangaize. The distance between Ménaka and Mangaize has in the new routes data decreased from 305 to approximately 200 kilometres. From Figure 19 it can

be derived that almost all of the increased discrepancy happens within the first 90 days of the conflict. This matches with the following statement by the UNHCR (2012):

"In Niger, most of the new arrivals are from Ménaka in Mali. Some have settled very close to the volatile border."

(UNHCR, 2012)

Most of the early refugees in Niger originate from Ménaka, which means that a shorter route between these locations, allows for earlier arrival. This is what the graph in Figure 19 shows as well. In reality, the current Ménaka-Mangaize route is most likely unavailable or takes longer to travel than simulated here, as the distance to the observed data increases in the new run. This could mean that factors other than the route length, such as the earlier mentioned border restrictions, play a more important role in the correct simulation of refugees in this area.

This same result is notable for Mentao and Bobo-Dioulasso, the two Burkina-Faso camps. In both cases, the overall refugee count has not changed much. The major change is the time of arrival of the refugees. For Mentao, the major spike starting around day 23 is caused by the conflicts erupting in Ansongo, Bourem and Gao, which start around this time. The earlier arrival of the refugees is caused by the decreased distance between Mentao and Douentza. Whereas the route is some 490 kilometres in the old model, this route is now some 270 kilometres in each season. The location of Douentza compared to Mentao and the conflict zones ensures that many refugees take the route through Douentza.

The reverse of this trend is true for Bobo-Dioulasso, where the refugees arrive a few days later in the new model, and the peak occurs some ten days later as well. This can be explained by the routes to Bobo-Dioulasso as well, which all have seen a significant increase in weighted distance. The routes from Mentao, Mopti and Ségou have increased by roughly one-hundred kilometres each (Table 17, Appendix 7.1).

Another notable trend in the data can be seen in the graphs for Fassala-Mbera and Niamey, where the difference in refugee arrivals for the two simulations increases steadily. These increases might be related to a combination of changed routes and the outbreak of conflicts. For Fassala-Mbera, the difference starts becoming visible around day 170. This matches with the outbreak of conflict in Bamako, the capital of Mali. This could result in a surge of refugees going to the nearest camp. In the new routes this is Fassala-Mbera, which is linked to Bamako through Ségou. The more direct link with the camp results in more arrivals in the camp. As the refugee numbers for Fassala-Mbera are so large compared to the others camps, the trend is also visible in the graph for total refugee arrivals.

The same trend in Niamey cannot be explained through the outbreak of a conflict however, as the dates do not match with the increase of numbers in the camp. However, it might be caused by other camps reaching capacity. The increase in disparity of refugee arrivals in Niamey starts around day 80 or 90. This is when the new route simulation starts to display an increase in arrivals compared to the old run. This matches with Mangaize reaching capacity around day 90 in the new run. The old run shows Mangaize reaching capacity around day 130, which is roughly when the increase in numbers in Niamey starts as well.

Tabareybarey shows little change between the two runs, which could be explained by the small changes in distance for the routes leading to this location. Interesting is that the new connection with Mentao seems to show little effect on the refugee numbers for the Niger camps of Tabareybarey and Niamey. This can be explained by the fact that refugees in these three locations are already in safety, and therefore do not choose to continue travelling. It is not affected by Mentao reaching capacity, as this occurs around the same time.

Changes in the refugee count for Abala might be caused by the new connection between Kidal and Ménaka, allowing for more direct travel to Abala from Kidal. This results in the earlier arrival of refugees.

4.3 Flee error analysis

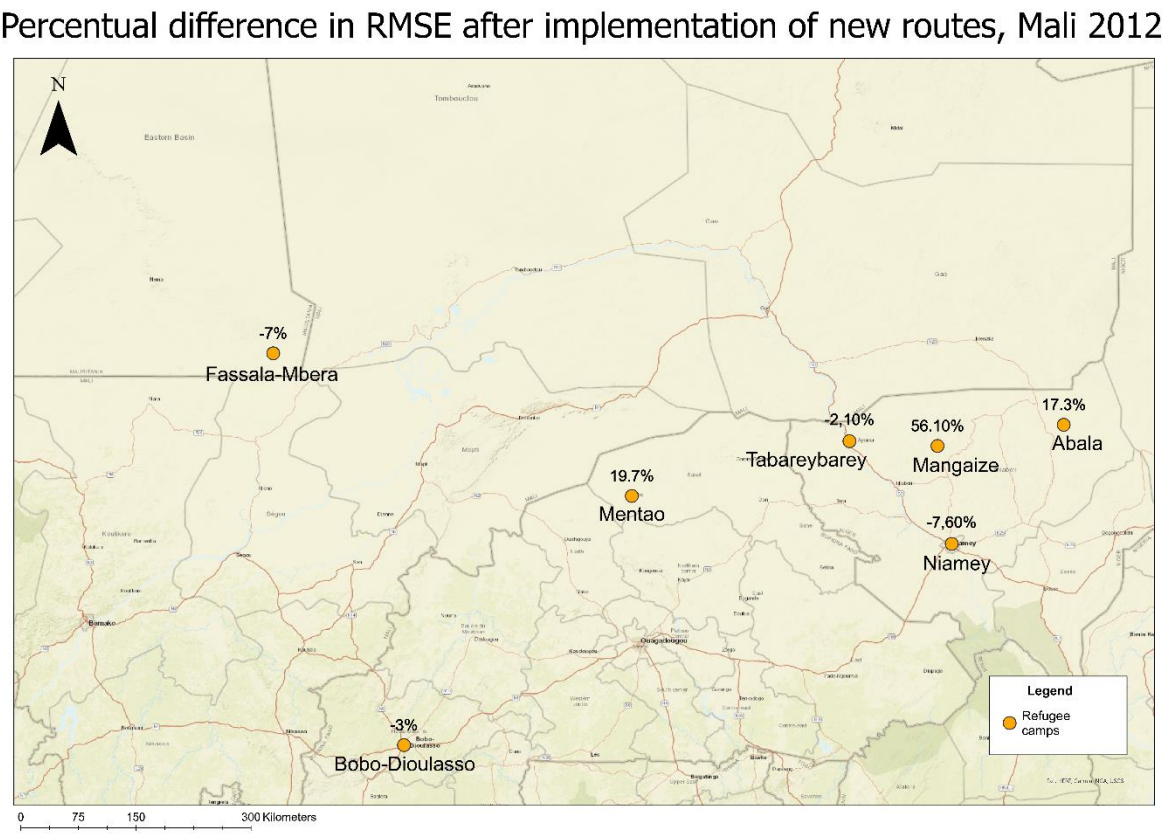

Figure 20: Spatial division of percentual differences in RMSE.

Four camps show a decrease in error as a result of the new routes, and the other three show an increase in error (Figure 20). However, the overall error has decreased by on average some 2200 refugees, which is a difference of around 16.5 percent. However, the total error reduction of 16.5 percent is mainly caused by the differences in the results for Fassala-Mbera. Due to the relative size of the Fassala-Mbera refugee camp, a difference in refugees here is projected directly to the total simulation results. In this case, if just the Fassala-Mbera error decreases due to changed routes, and other locations see an increase in error, the total error might still decrease. If the impact of the changed routes on the error per location is to be tested, all locations should have the same weight. This can be done by taking the average of the '%-difference' column in Table 19 (Appendix 7.3). Including the total difference, the error between old and new simulations increases by roughly 7%. Excluding the total difference, this number is increased to 10%. This method shows that the relative difference caused by the changes in routes, might actually increase the error, and negatively impact the accuracy of the model.

The normalized errors (NRMSE) for some locations are higher than others (Table 20, Appendix 7.4). Mainly the errors for Niamey, Tabareybarey and Bobo-Dioulasso stand out, in both simulations. These errors are caused by a discrepancy between the simulated data and the observed data. A difference in error indicates an increase or decrease in this discrepancy between the old and new runs. The largest differences occur in Mangaize, Mentao, Niamey and over the total simulation. The ways in which the results for these and other camps have changed, and why this is the case, is discussed in section 4.2. The reasons for the changes in absolute refugee numbers are the same for the changes in RMSE.

To inspect the influence of the temporal fluctuations in routes, the NRMSE is calculated seasonally per location as well (Table 21, Appendix 7.5; Figure 21).

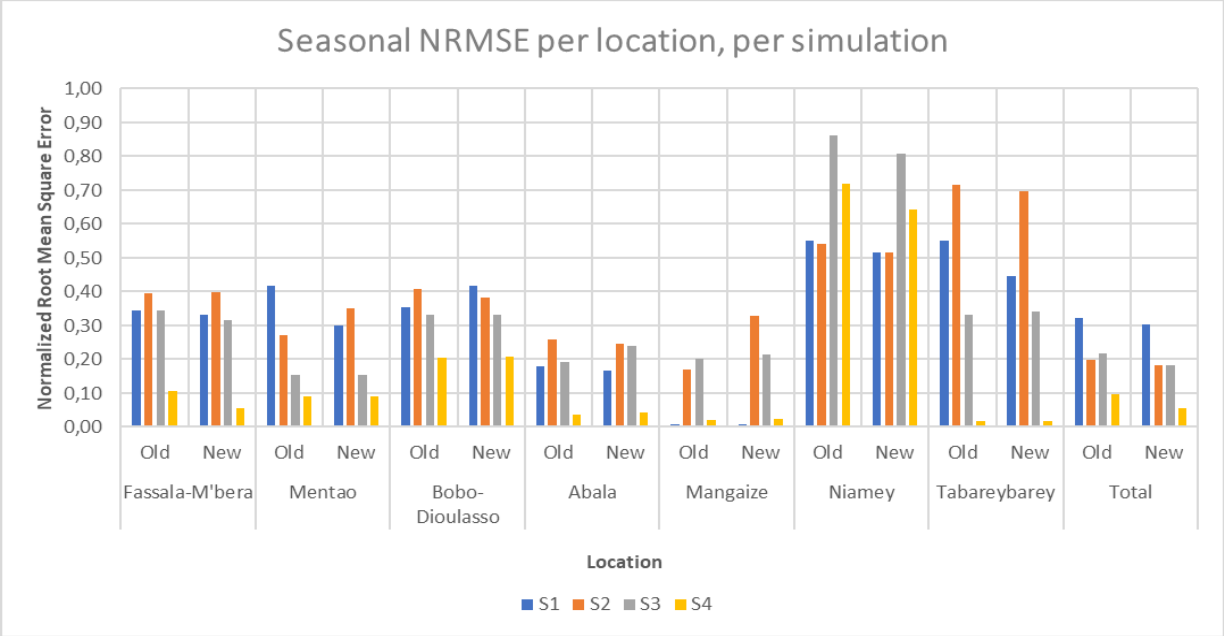

Figure 21: RMSE normalized per season.

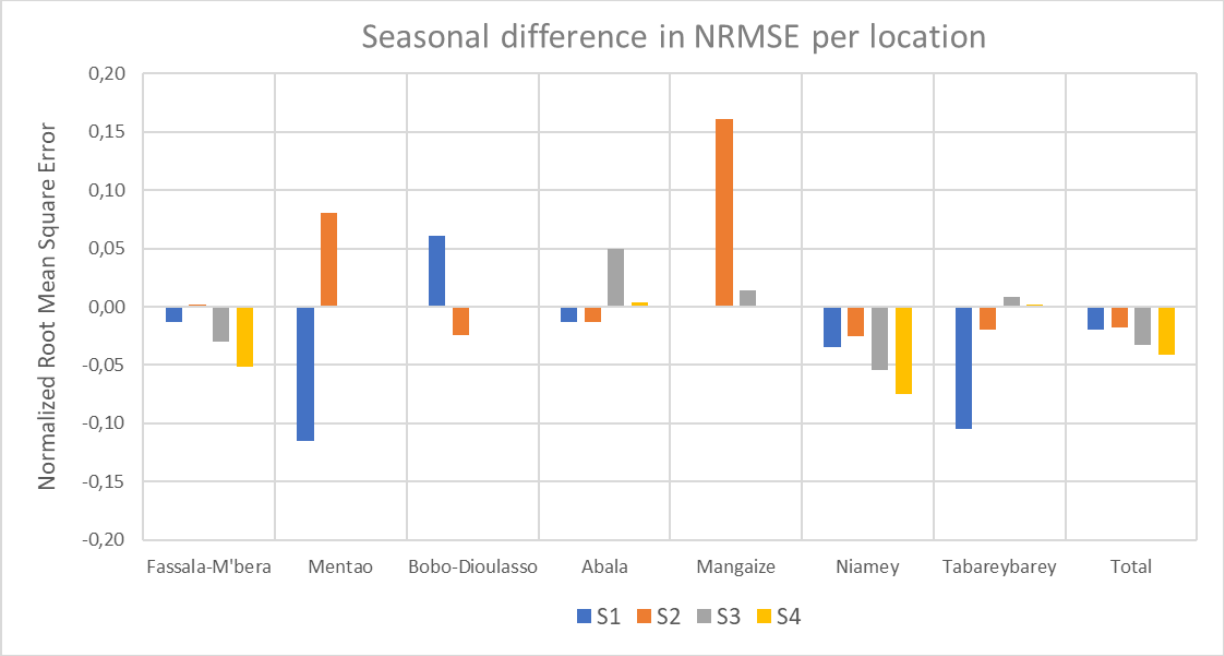

Figure 22: Seasonal changes in NRMSE between two simulations, per location.

On the data in Table 21 (Appendix 7.5), the seasonal average is calculated, and is displayed in the lower row. This metric shows that season 2 is overall the season with the highest error, with an average of 0.38 between the two runs. Season 4 has the lowest error, with an average of 0.14. Season 1 and 3 are somewhat similar, around 0.33. The seasonal average shows as well that the error has decreased for each season in the new run, except season 2. Figure 21 shows which locations have relatively high or low errors. In this, Niamey stands out as the location with the largest error. To inspect these seasonal changes between the old and new runs, the differences per location per season are visualized in Figure 22.

Figure 21 highlights the differences in NRMSE per season. For Fassala-Mbera, an overall decrease in error can be seen, the degree of which increases steadily for the duration of the simulation, with an exception of season 2. This means that the new run becomes more accurate in comparison to the old

run as the simulation progresses. This same exact pattern, including the season 2 exception, is visible for Niamey and the total. Mentao shows a different pattern, with a large decrease in error in the first season and a large increase, compared to the old run, in the second season. Table 21 (Appendix 7.5) shows that the new simulation is more stable, fluctuating between 0.3 and 0.35 NRMSE in the first two seasons, whereas in the old run this fluctuation is larger, between 0.42 and 0.27. For Mangaize, an increase in season 2 is visible, while other seasons remain stable. Table 20 (Appendix 7.4) shows an increase in NRMSE in Mangaize of some 50%. From Figure 22 it can be derived that this change happens almost entirely in season 2.

Overall, most error is concentrated in season 2 and 3. Error in season 1 is lower, partially due to the border closure mechanic in Flee. This results in the error being near zero for some locations, in the beginning of the simulation. The same effect is caused by some camps reaching capacity in season 4. Season 4 has the lowest average error, as several camps reach capacity for a significant part of this season, bringing the error near to zero again. This effect is noteworthy, as more often in agent-based modelling, the error increases towards the end of the simulation. Kieu et al. (2020) state that:

"(..) as the simulation progresses, the prediction rapidly diverges from reality owing to underlying uncertainties."

(Kieu et al., 2020)

This is not the case in Flee, due to the capacity variable applied to camps, meaning that all camps drift towards a lower error, as they gradually 'fill'. The result of these effects is that it might not be meaningful to take into account the errors of the first and the last season, as they do not reflect the accuracy of the models' methods for assigning refugees to camps. From this point of view it is only meaningful to compare the differences between the runs in season 2 and 3. In this case, the change in error due to the changing of routes is minimal: the NRMSE increases on average by 0.01 between the old and the new routes.

On the results of both simulation runs, the averaged relative difference is calculated. This measure is described in section 3.8. For the simulation runs with the original routes, the ARD is 0.361. For the runs with the new routes, this is 0.345. This difference indicates an improvement in accuracy, as can be seen in the overall RMSE as well. However, the improvement is relatively small, which underlines the conclusion that the effective reduction in error caused by the change in routes is small. These results lead to the conclusion that the main issue of Flee does not lie with the routes. Other factors, for example political or emotional factors, such as border restrictions and the attractiveness of cities, seem to play a larger role than the distance of routes. This hypothesis is supported by the study performed by Suleimenova & Groen (2020), whose findings indicate change induced by the implementation of additional border restriction mechanics, and the reduction of camp capacity for a case study in South Sudan. Looking for example at the graphs of Niamey, Tabareybarey and Abala in Figure 19: despite differences between runs caused by the changing of routes, the overarching inaccuracies of the simulation remain. These issues, such as the underprojection of refugees in Niamey, cannot be solved by changing the routes. To increase the accuracy of Flee, the focus should not lie with changing of routes, but with implementing other dynamics that might influence refugee behaviour.

4.4 Limitations and Recommendations

The methods in this study are prone to limitations, which might affect the results and the interpretation thereof. In this section the most influential of these limitations is addressed.

First, the representation of the physical environment. To create the cost raster, and subsequently the routes, the physical environment of Mali is mapped in raster data, and represented as speed multiplier values. In doing this, the environment of Mali is reduced to several physical features: relief, soil, drainage and infrastructure. This reduction results in not taking into account many other aspects of the environment, for example vegetation, or more broadly surface cover. The presence of trees, brushes, rocks or other obstructions certainly influences driving routes and speeds. However, the choice is made to not take these into account in this study, due to time restrictions. Furthermore, this feature type is chosen to be left out as it was deemed the least influential for travel in Northern Mali.

The second limitation is induced by time constraints and pertains to the calibration of the routes. In section 4.1 it is shown that the weighted distances of the routes are overall lower than reality. This is caused by an underestimation of the duration required to travel a route. The duration, or travel time, is based on the cost raster and the least cost path operation. An underestimation of the duration is caused by an underestimation of the speed multipliers, representing the resistance of a physical feature, and the maximum speed. Adapting these values to make the cost raster and the routes more realistic is part of the calibration stage of the study. Usually, calibration is an iterative process, meaning repetition is built into the methodology. However, in this study time constraints meant that the calibration of these values could only be performed once, limiting the ability to adjust the values. More iterations of the calibration phase could have resulted in more accurate results.

The final limitation pertains to the quality of the observed data used as comparison (UNHCR, 2021). D. Groen (personal communication, February 2022) stated that:

"Keep in mind that the UNHCR data is not exactly of good quality, so it makes little sense to discuss or interpret extensively the mismatches on the individual camp level."

The lack in data quality can be observed for example in Figure 19, in the Niamey graph. Here, the observed data shows steady increases and sudden changes in refugee numbers. This is most likely not the result of actual daily measurements, but and extrapolation of a smaller number of measurements. This means that comparing the simulated data to the UNHCR data on a day-to-day basis, or interpreting the different fluctuations in refugee numbers between the observed and the simulated data, might not be completely meaningful.

Besides these limitations, several assumptions are made throughout the study as well. These are described at a relevant section, but are listed here as well:

1. *Refugee travel is exclusively vehicular.*

This assumption is made, as the original Flee model, to which the results of this study are compared, applied this as well. Furthermore, due to the great distances and harsh conditions in Mali, non-vehicular travel becomes a dangerous and often deadly ordeal. This is confirmed by B. Ooink (personal communication, September 2021).

2. *Seasonal changes of Niger river water level and the effect on infrastructure.*

It is assumed that the seasonal changes in water level in the Niger river affect the accessibility of river crossings in a binary way. Fordable areas are not accessible in seasons one and four, due to high river levels. Ferries are not accessible in seasons two and three, when the water level is at its lowest. This classification is an oversimplified version of reality. In some cases, the accessibility classification might not be an accurate representation of reality, leading to a decrease in accuracy of results.

3. *Seasonal continuity of speed multiplier values.*

It is assumed that the speed multiplier values for land cover, infrastructure and slope remain the same throughout the seasons. In reality, these might change due to changes in moisture content for example. However, such detailed information on the resistance of physical features would be specific for the study area, and is not available for Mali.

For follow-up studies it is recommended to perform several calibrations of the routes data, before applying it into Flee. Furthermore, a more detailed look into the resistance values, by for example a field test, is recommended as well.

5. Conclusion

The general aim of this study is identifying to what extent aspects of the physical environment affect refugee flight behaviour, and if the implementation thereof in Flee would improve its simulation of refugee behaviour. The secondary aim is the improvement of the accuracy of the Flee model.

This is approached by creating a representation of the physical environment in the form of a raster. Four different representations are made to represent seasonal changes in the environment. Physical features relevant to refugee travel are selected and assigned speed multiplier values, based on the resistance these features offer to vehicles. This value represents a limitation to maximum speed. The resulting raster values are multiplied by a maximum speed, creating a speed raster. This raster is converted into a cost raster, which allows for the plotting of least-cost paths through the raster. The resulting routes are implemented into the Flee model to test for improvements. The case study for this study is the 2012 conflict in Mali.

The main research question for the study is posed as follows: **'To what extent does the physical environment determine flight routes for refugees?'**. This question is answered through three sub questions:

To what extent does a representation of the physical environment approach accurate refugee travel times and distances?

The results show that the plotted routes quite accurately follow expected patterns and major roads where possible, indicating that the hierarchy in speed multiplier values is fairly accurate. The travel time of the routes and subsequently the weighted distances, are lower than reality, indicating that the speed multiplier values and the maximum speed are more optimistic than real-world travel.

What is the effect of the integration of the cost raster data on the spatial aspect of the projected refugee destinations of the Flee model's simulations?

Overall, the error for the model is reduced through the implementation of the new routes. However, this is caused mainly by the relative size of the Fassala-Mbera camp. The error adjusted for the size of the camps, allowing for equal comparison of the effect of routes, even shows an increase in error of 7% – 10%.

What is the effect of the integration of the cost raster data on the temporal aspect of the projected refugee destinations of the Flee model's simulations?

Temporally, most error is concentrated in seasons two and three. The error for seasons one and four is not representative of the model's capacity for simulation, as the results are distorted by the border closure and camp capacity mechanics in Flee. The difference in normalized error for seasons two and three is negligible.

These answers result in the answering of the main research question: the physical environment does not have a major impact on refugee flight behaviour, as it is represented in the Flee model. Although the adjusted routes do induce change, this change is not unambiguously positive or negative. Furthermore, the main issue of Flee's inaccuracies does not lie with the routes. Other factors, for example political or emotional factors, such as border restrictions and the attractiveness of cities, seem to play a larger role in the model's error than the distance of routes. It is therefore concluded that the secondary aim of this study, the improvement of the Flee model, is not achieved. To reduce the errors in Flee, the focus should not lie with the changing of routes, but with implementing other dynamics that might influence refugee behaviour.

6. Bibliography

Abel, G. J., Brottrager, M., Crespo Cuaresma, J., & Muttarak, R. (2019). Climate, conflict and forced migration. *Global Environmental Change*, *54*, 239–249. https://doi.org/10.1016/j.gloenvcha.2018.12.003

ACLED. (2021). *ACLED Data Dashboard* . https://acleddata.com/dashboard/#/dashboard

Anastasiadis, P., Gogolenko, S., Papadopoulou, N., Lawenda, M., Arabnejad, H., Jahani, A., Mahmood, I., & Groen, D. (2021). P-Flee: An Efficient Parallel Algorithm for Simulating Human Migration. *2021 IEEE International Parallel and Distributed Processing Symposium Workshops, IPDPSW 2021 - In Conjunction with IEEE IPDPS 2021*, *April*, 1008–1011. https://doi.org/10.1109/IPDPSW52791.2021.00159

Anderson, J., Chaturvedi, A., & Cibulskis, M. (2007). Simulation tools for developing policies for complex systems: Modeling the health and safety of refugee communities. *Health Care Management Science*, *10*(4), 331–339. https://doi.org/10.1007/s10729-007-9030-y

Andersson, J. C. M., Ali, A., Arheimer, B., Gustafsson, D., & Minoungou, B. (2017). Providing peak river flow statistics and forecasting in the Niger River basin. *Physics and Chemistry of the Earth, Parts A/B/C*, *100*, 3–12. https://doi.org/10.1016/J.PCE.2017.02.010

Baylot, E. A., Gates, B. Q., Green, J. G., Richmond, P. W., Goerger, N. C., Mason, G. L., Cummins, C. L., & Bunch, L. S. (2005). *Standard for Ground Vehicle Mobility*.

Bencherif, A., Campana, A., & Stockemer, D. (2020). Lethal Violence in Civil War: Trends and Micro-Dynamics of Violence in the Northern Mali Conflict (2012-2015). *Studies in Conflict and Terrorism*. https://doi.org/10.1080/1057610X.2020.1780028

Bianchi, C., Cirillo, P., Gallegati, M., Vagliasindi, P. A., Bianchi, C., Gallegati, M., & Vagliasindi, P. A. (2007). *Validating and Calibrating Agent-Based Models: A Case Study*. *30*, 245–264. https://doi.org/10.1007/s10614-007-9097-z

Bonabeau, E. (2002). Agent-based modeling: Methods and techniques for simulating human systems. In *Proceedings of the National Academy of Sciences of the United States of America* (Vol. 99, Issue SUPPL. 3). https://doi.org/10.1073/pnas.082080899

Campos, C. V., Suleimenova, D., & Groen, D. (2019). *A Coupled Food Security and Refugee Movement Model for the South Sudan Conflict*. https://www.aljazeera.com/indepth/features/2013/12/south-sudan

Casse, C., Gosset, M., Peugeot, C., Pedinotti, V., Boone, A., Tanimoun, B. A., & Decharme, B. (2015). Potential of satellite rainfall products to predict Niger River flood events in Niamey. *Atmospheric Research*, *163*, 162–176. https://doi.org/10.1016/J.ATMOSRES.2015.01.010

Castle, C. J. E., & Crooks, A. T. (2006). Principles and concepts of agent-based modelling for developing geographical simulations. *CASA Working Paper Series*, *110*(0), 60. http://www.casa.ucl.ac.uk/publications/workingPaperDetail.asp?ID=110

Chai, T., & Draxler, R. R. (2014). Root mean square error (RMSE) or mean absolute error (MAE)?-Arguments against avoiding RMSE in the literature. *Geosci. Model Dev*, *7*, 1247–1250. https://doi.org/10.5194/gmd-7-1247-2014

Choi, Y., Um, J.-G., & Park, M.-H. (2013). *Cartography and Geographic Information Science Finding least-cost paths across a continuous raster surface with discrete vector networks Finding least-cost paths across a continuous raster surface with discrete vector networks*. https://doi.org/10.1080/15230406.2013.850837

Crooks, A. T., & Heppenstall, A. J. (2011). *Introduction to Agent-Based Modelling*. https://doi.org/10.1007/978-90-481-8927-4_5

D'errico, M., Bori, A., & Campos, A. P. de la O. (2021). Resilience and conflict: Evidence from mali. *Sustainability (Switzerland)*, *13*(18). https://doi.org/10.3390/SU131810444

De Kock, C. (2019). *A framework for modelling conflict-induced forced migration according to an*

agent-based approach. https://scholar.sun.ac.za:443/handle/10019.1/107038

Eid, A. N. M., Olatubara, C. O., Ewemoje, T. A., El-Hennawy, M. T., & Farouk, H. (2020). Inland wetland time-series digital change detection based on SAVI and NDWI indecies: Wadi El-Rayan lakes, Egypt. *Remote Sensing Applications: Society and Environment*, *19*. https://doi.org/10.1016/j.rsase.2020.100347

Gallant, A. L. (2015). The Challenges of Remote Monitoring of Wetlands. *U.S. Geological Survey*, *7*, 10938–10950. https://doi.org/10.3390/rs70810938

Gambill, D. R., Wall, W. A., Fulton, A. J., & Howard, H. R. (2016). Predicting USCS soil classification from soil property variables using Random Forest. *Journal of Terramechanics*, *65*, 85–92. https://doi.org/10.1016/J.JTERRA.2016.03.006

GIS Ag Maps - Sentinel-2 Surface Reflectance Tutorial. (n.d.). Retrieved November 18, 2021, from https://www.gisagmaps.com/s2-atmospheric-correction

Gislason, P. O., Benediktsson, J. A., & Sveinsson, J. R. (2005). Random Forests for land cover classification. *Department of Electrical and Computer Engineering*, *2*(6). https://reader.elsevier.com/reader/sd/pii/S0167865505002242?token=5D0B53237D37D967CD86A8D6CBBF37A4F5E8C4CE48E38DAD5E94752C5FE01F6955D035777F1CACC9A46808067616E63F&originRegion=eu-west-1&originCreation=20211201134216

Groen, D. (2016). Simulating refugee movements: Where would you go? *Procedia Computer Science*, *80*, 2251–2255. https://doi.org/10.1016/j.procs.2016.05.400

Guo, X., & Lu, H. (2009). Research on Trafficability of Engineering Vehicles in Wetland. *Second International Conference on Intelligent Computation Technology and Automation*, 732–735.

Hubáček, M., & Rybansky, M. (2013). *THE CROSS-COUNTRY MOVEMENT IN SANDY AREAS Modeling the impact of meteorological conditions on the carrying capacity of soils View project NATURENVIR View project*. https://www.researchgate.net/publication/268818436

Kieu, L.-M., Malleson, N., & Heppenstall, A. (2020). *Dealing with uncertainty in agent-based models for short-term predictions*. https://doi.org/10.1098/rsos.191074

Lefebvre, G., Davranche, A., Willm, L., Campagna, J., Redmond, L., Merle, C., Guelmami, A., & Poulin, B. (2019). Introducing WIW for detecting the presence of water in wetlands with landsat and sentinel satellites. *Remote Sensing*, *11*(19). https://doi.org/10.3390/RS11192210

Lounnas, D. (2013). The Regional Fallouts of the French Intervention in Mali. *Mediterranean Politics*, *18*(2), 325–332. https://doi.org/10.1080/13629395.2013.799351

Macal, C. M. (2016). Everything you need to know about agent-based modelling and simulation. *Journal of Simulation*, *10*(2), 144–156. https://doi.org/10.1057/jos.2016.7

Mach, K. J., Kraan, C. M., Neil Adger, W., Buhaug, H., Burke, M., Fearon, J. D., Field, C. B., Hendrix, C. S., Maystadt, J.-F., O'loughlin, J., Roessler, P., Scheffran, J., Schultz, K. A., & Von Uexkull, N. (2019). Climate as a risk factor for armed conflict. *Nature*, *571*. https://doi.org/10.1038/s41586-019-1300-6

Mahdavi, S., Salehi, B., Granger, J., Amani, M., Brisco, B., & Huang, W. (2017). *Remote sensing for wetland classification: a comprehensive review*. https://doi.org/10.1080/15481603.2017.1419602

Malm, F. (2019). One hundred years of cross-country mobility prediction in Germany. *Geological Society, London, Special Publications*, *473*(1), 297–306. https://doi.org/10.1144/SP473.7

McFeeters, S. K. (1996). The use of the Normalized Difference Water Index (NDWI) in the delineation of open water features. *Https://Doi.Org/10.1080/01431169608948714*, *17*(7), 1425–1432. https://doi.org/10.1080/01431169608948714

Migrants Refugees. (2020). *Migration Profile MALI*. www.migrants-refugees.va

Murekatete, R. M., & Shirabe, T. (2020). *An experimental analysis of least-cost path models on ordinal-scaled raster surfaces*. https://doi.org/10.1080/13658816.2020.1753204

Özelkan, E. (2020). Water Body Detection Analysis Using NDWI Indices Derived from Landsat-8 OLI. *Polish Journal of Environmental Studies*, *29*(2), 1759–1769. https://doi.org/10.15244/PJOES/110447

Pavelic, P., Giordano, M., Keraite, B., Ramesh, V., & Rao, T. (2012). *Groundwater Availability and Use in Sub-Saharan Africa: A Review of 15 Countries*. International Water Management Institute (IWMI). http://citeseerx.ist.psu.edu/viewdoc/download?doi=10.1.1.432.8873&rep=rep1&type=pdf#page=103

R4Sahel. (n.d.). *Situation Sahel Crisis*. Retrieved October 5, 2021, from https://r4sahel.info/en/situations/sahelcrisis/location/8695

Ramm, F. (2021). *OpenStreetMap Data in Layered GIS Format*. www.openstreetmap.org

Rokni, K., Ahmad, A., Selamat, A., & Hazini, S. (2010). Water Feature Extraction and Change Detection Using Multitemporal Landsat Imagery. *Remote Sens*, *6*, 4173–4189. https://doi.org/10.3390/rs6054173

Rundquist, D. C., Narumalani, S., & Narayanan, R. M. (2001). *A review of wetlands remote sensing and defining new considerations*. *20*(3), 207–226. https://www.tandfonline.com/doi/pdf/10.1080/02757250109532435

Rybanský, M. (2003). Effect of the Geographic Factors on Cross Country Movement. *Proceedings of the 21st International Cartographic Conference (ICC)*, 10–16.

Rybansky, M., Hofmann, A., Hubacek, M., Kovarik, V., & Talhofer, V. (2015). Modelling of cross-country transport in raster format. *Environmental Earth Sciences*, *74*(10), 7049–7058. https://doi.org/10.1007/s12665-015-4759-y

Sarp, G., & Ozcelik, M. (2017). Water body extraction and change detection using time series: A case study of Lake Burdur, Turkey. *Journal of Taibah University for Science*, *11*(3), 381–391. https://doi.org/10.1016/j.jtusci.2016.04.005

Searle, C., & Van Vuuren, J. H. (2021). Modelling forced migration: A framework for conflict-induced forced migration modelling according to an agent-based approach. *Computers, Environment and Urban Systems*, *85*, 101568. https://doi.org/10.1016/j.compenvurbsys.2020.101568

Shaw, S. (2013). Fallout in the Sahel: the geographic spread of conflict from Libya to Mali. *Canadian Foreign Policy Journal*, *19*(2), 199–210. https://doi.org/10.1080/11926422.2013.805153

Shoop, S., Affleck, R., Collins, C., Larsen, G., Barna, L., & Sullivan, P. (2005). Maneuver analysis methodology to predict vehicle impacts on training lands. *Journal of Terramechanics*, *42*, 281–303.

Sokolowski, J. A., Banks, C. M., & Hayes, R. L. (2015). Modeling population displacement in the Syrian city of Aleppo. *Proceedings - Winter Simulation Conference*, *2015-January*, 252–263. https://doi.org/10.1109/WSC.2014.7019893

Sokolowski, J. A., Banks, C. M., & Modeling, V. (2014). *A Methodology for Environment and Agent Development to Model Population Displacement KEY WORDS population displacement, early warning model, United Nations Human Rights Council (UNHRC), ABM environment matrix, ABM agent matrix*.

Stillwell, J. (2005). Inter-regional migration modelling - a review and assessment. *European Regional Science Association (ERSA)*, *23*(27), 23–27. http://hdl.handle.net/10419/117857www.econstor.eu

Suleimenova, D., Bell, D., & Groen, D. (2017). A generalized simulation development approach for predicting refugee destinations. *Scientific Reports*, *7*(1). https://doi.org/10.1038/s41598-017-13828-9

Suleimenova, D., & Groen, D. (2020). How policy decisions affect refugee journeys in South Sudan: A study using automated ensemble simulations. *Jasss*, *23*(1). https://doi.org/10.18564/jasss.4193

Suvinen, A. (n.d.). *TERRAIN MOBILITY MODEL AND DETERMINATION OF OPTIMAL OFF-ROAD ROUTE*.

The World Bank. (2021). *Refugee population by country or territory of asylum - Mali | Data*. https://data.worldbank.org/indicator/SM.POP.REFG?end=2020&locations=ML&start=2012&type=shaded&view=chart

UNHCR - UNHCR addresses needs of 20,000 forced to flee violence in Mali. (2012, February 7). https://www.unhcr.org/news/makingdifference/2012/2/4f312a219/unhcr-addresses-needs-20000-forced-flee-violence-mali.html

UNHCR. (n.d.). *Country - Mali*. Retrieved October 5, 2021, from https://data2.unhcr.org/en/country/mli

UNHCR. (2021). Global Trends: Forced Displacement in 2020. *Unhcr*, 72.

Zolberg, A. R., Suhrke, A., & Aguayo, S. (1986). International Factors in the Formation of Refugee Movements. *International Migration Review*, *20*. https://heinonline.org/HOL/Page?handle=hein.journals/imgratv20&id=417&div=&collection=

7. Appendix

7.1 Route distances

Table 17: Route weighted distance changes. Average Difference column is calculated over the seasonal mean.

Location A	Location B	New distance, season 1	New distance, season 2	New distance, season 3	New distance, season 3	Old distance	Average Difference (%)
Abala	*Menaka*	216,21	216,21	216,21	216,21	172	25,7%
Abala	*Niamey*	275,27	275,27	275,27	275,27	253	8,8%
Ansongo	*Gao*	124,41	120,33	120,33	124,41	100	22,4%
Ansongo	*Menaka*	271,07	271,07	271,07	271,07	191	41,9%
Bobo Dioulasso	*Bamako*	628,28	628,28	628,28	628,29	-	
Bobo Dioulasso	*Mentao*	535,99	535,99	535,99	535,99	475	12,8%
Bobo Dioulasso	*Mopti*	534,76	534,65	534,76	535,28	462	15,8%
Bobo Dioulasso	*Segou*	479,59	470,33	483,49	479,6	376	27,2%
Bourem	*Gao*	104,46	104,46	104,46	104,46	97	7,7%
Bourem	*Timbuktu*	455,05	455,05	455,05	455,05	314	44,9%
Douentza	*Gao*	458,69	458,69	458,69	458,69	397	15,5%
Douentza	*Konna*	129,17	129,17	129,17	129,17	121	6,8%
Douentza	*Mentao*	271,64	271,64	271,64	271,64	487	-44,2%
Douentza	*Timbuktu*	274,18	993,6	1017,87	288,13	-	
Goundam	*Diré*	40,34	40,28	40,28	40,34	42	-4,0%
Goundam	*Niafunké*	96,24	96,24	96,24	96,24	78	23,4%
Goundam	*Timbuktu*	99,3	99,3	99,3	99,3	85	16,8%
Kidal	*Ansongo*	527,64	523,57	523,57	527,64	-	
Kidal	*Bourem*	329,59	329,59	329,59	329,59	308	7,0%
Kidal	*Gao*	410	410	410	410	-	
Kidal	*Menaka*	420,6	420,6	420,6	420,6	-	
Konna	*Mopti*	75,48	75,48	75,48	79,98	70	9,4%
Konna	*Niafunké*	573,86	929,43	945,46	589,68	153	396,5%
Konna	*Timbuktu*	392,15	1122,52	1140,15	406,1	303	152,6%
Léré	*Fassala-Mbera*	155,67	155,67	155,67	155,67	98	58,8%
Léré	*Niafunké*	153,06	139,62	139,63	139,63	140	2,1%
Léré	*Ténenkou*	232,57	232,57	232,57	232,57	295	-21,2%
Mangaize	*Abala*	259,78	259,78	259,78	259,78	256	1,5%
Mangaize	*Menaka*	200,57	200,57	200,57	200,57	305	-34,2%
Mangaize	*Niamey*	171,97	171,97	171,97	171,97	159	8,2%
Mangaize	*Tabareybarey*	174,23	174,06	174,06	174,23	217	-19,7%
Mentao	*Ansongo*	445,25	563,68	564,57	448,09	-	
Mentao	*Mopti*	386,67	386,67	386,67	391,18	360	7,7%
Mentao	*Niamey*	512,6	512	510,45	512,6	-	
Mentao	*Tabareybarey*	580,7	418,16	554,17	583,54	-	
Niafunké	*Ténenkou*	380,14	354,52	354,27	369,66	308	18,4%
Segou	*Bamako*	269,04	269,04	269,04	269,04	240	12,1%
Segou	*Fassala-Mbera*	387,66	387,66	387,66	387,72	-	
Segou	*Mopti*	342,47	365,09	385,74	373,5	401	-8,6%
Segou	*Ténenkou*	255,24	255,85	256,59	255,87	228	12,2%
Tabareybarey	*Abala*	415,11	415,11	415,11	415,11	412	0,8%
Tabareybarey	*Ansongo*	161,63	161,63	161,63	161,63	148	9,2%
Tabareybarey	*Menaka*	346,66	346,66	346,66	346,66	361	-4,0%
Tabareybarey	*Niamey*	224,69	224,69	224,69	224,69	205	9,6%

7.2 Route travel times

Table 18: Average simulated and observed travel times for a selection of locations connected by roads.

Name1	Name2	Average simulated travel time (all seasons)	Observed travel time (Google Maps)	%-difference (absolute)
Bamako	Ségou	~3.4 hours	~3.5 hours	2.9%
Bamako	Bobo-Dioulasso	~7.8 hours	~9.3 hours	16.1%
Ségou	Bobo-Dioulasso	~6 hours	~6.5 hours	7.7%
Ségou	Mopti	~4.8 hours	~5.5 hours	12.7%
Mopti	Bobo-Dioulasso	~6.7 hours	~7.5 hours	10.7%
Douentza	Gao	~5.7 hours	~7.75 hours	26.5%

7.3 Root Mean Square Error

Table 19: RMSE average values over ten runs. In the 'Difference' and '%-difference' columns, a negative value indicates an improvement in the average RMSE of the camp.

Location	Old route mean RMSE	New route mean RMSE	Difference	%-difference
Fassala-Mbera	14211	13215	-996	-7,0%
Mentao	1268	1517	249	+19,7%
Bobo-Dioulasso	632	613	-19	-3,0%
Abala	1491	1749	258	+17,3%
Mangaize	477	745	268	+56,1%
Niamey	4026	3721	-305	-7,6%
Tabareybarey	2696	2640	-57	-2,1%
Total	13518	11292	-2226	-16,5%

7.4 Normalized Root Mean Square Error

Table 20: NRMSE average values over ten runs.

Location	Old route mean normalized RMSE	New route mean normalized RMSE	Difference
Fassala-Mbera	0.26	0.24	-0.023
Mentao	0.18	0.22	0.035
Bobo-Dioulasso	0.31	0.30	-0.006
Abala	0.13	0.15	0.021
Mangaize	0.14	0.22	0.080
Niamey	0.62	0.57	-0.047
Tabareybarey	0.43	0.42	-0.008
Total	0.15	0.13	-0.025

7.5 NRMSE seasonal analysis

Table 21: RMSE normalized per season.

Location	Normalized Root Mean Square Error							
	Season 1		***Season 2***		***Season 3***		***Season 4***	
	Old	*New*	*Old*	*New*	*Old*	*New*	*Old*	*New*
Fassala-Mbera	0.34	0.33	0.40	0.40	0.34	0.31	0.11	0.06
Mentao	0.42	0.30	0.27	0.35	0.15	0.16	0.09	0.09
Bobo-Dioulasso	0.36	0.42	0.41	0.38	0.33	0.33	0.21	0.21
Abala	0.18	0.17	0.26	0.25	0.19	0.24	0.04	0.04
Mangaize	0.01	0.01	0.17	0.33	0.20	0.21	0.02	0.02
Niamey	0.55	0.52	0.54	0.52	0.86	0.81	0.72	0.64
Tabareybarey	0.55	0.44	0.72	0.70	0.33	0.34	0.02	0.02
Total	0.32	0.30	0.20	0.18	0.22	0.18	0.10	0.06
Seasonal average	0.34	0.31	0.37	0.39	0.33	0.32	0.16	0.14

7.6 File structure of added file

Along with this thesis, a .zip file is provided that includes several files used in the study. These files include datasets, Google Earth Engine scripts and ArcGIS Pro ModelBuilder tools. The raw data could not be added in this way, as the file size is several hundreds of gigabytes. The file structure:

A – GEE scripts *includes the code used for the creation of several datasets in Google Earth Engine*

NDWIcreation.docx;

ROCKYAREAScreation.docx;

SLOPEcreation.docx;

WiWcreation.docx

B – Routes *includes the results from the route creation, in weighted distances, and a change comparison*

RoutesTables

RoutesFinal.xlsx;

RoutesTableS1.csv;

RoutesTableS2.csv;

RoutesTableS3.csv;

RoutesTableS4.csv

DistanceChangeAnalysis.xlsx

C – FleeOld *includes Flee results from ten runs with the old routes*

Out1.csv;

(…)

Out10.csv

D – FleeNew *includes Flee results from ten runs with the new routes*

Out1_new.csv;

(…)

Out10_new.csv

E – FleeAnalysis *includes the main files used for the analysis of the Flee results and the creation of graphs and tables.*

RefugeeAverageComparison.xlsx

RMSEanalysis.xlsx

Z – ArcGIS Modelbuilders *includes a toolbox of the main ModelBuilder models used in the study. The toolbox file, .atbx, can only be opened in ArcGIS Pro. The ModelBuilder tools are also converted to .py files, for alternative interpretation. The ModelBuilders include the Cost Raster creation, the Cost Distance and Backlink creation, and the Least-Cost Path creation.*

ArcGISModelBuilderPython

Thesis – ArcGIS ModelBuilder.atbx